



## Article

# Chlorophyll-a Detection Algorithms at Different Depths Using In Situ, Meteorological, and Remote Sensing Data in a Chilean Lake

Lien Rodríguez-López <sup>1,\*</sup> , Denisse Alvarez <sup>2</sup> , David Bustos Usta <sup>3</sup>, Iongel Duran-Llacer <sup>4</sup> , Lisandra Bravo Alvarez <sup>5</sup> , Nathalie Fagel <sup>6</sup>, Luc Bourrel <sup>7</sup>, Frederic Frappart <sup>8</sup> and Roberto Urrutia <sup>9</sup>

<sup>1</sup> Facultad de Ingeniería, Arquitectura y Diseño, Universidad San Sebastián, Lientur 1457, Concepcion 4030000, Chile

<sup>2</sup> Centro Bahía Lomas, Facultad de Ciencias, Universidad Santo Tomás, Concepcion 4030000, Chile; dalvarezsa@usantotomas.cl

<sup>3</sup> Facultad de Oceanografía, Universidad de Concepción, Concepcion 4030000, Chile; davidbustos@udec.cl

<sup>4</sup> Hémera Centro de Observación de la Tierra, Facultad de Ciencias, Ingeniería y Tecnología, Universidad Mayor, Camino La Pirámide 5750, Santiago 8580745, Chile; iongel.duran@umayor.cl

<sup>5</sup> Department of Electrical Engineering, Universidad de Concepción, Edmundo Larenas 219, Concepcion 4030000, Chile; lisanbravo@udec.cl

<sup>6</sup> UR Argile, Geochimie et Environment Sedimentary (AGEs), Geology Department, University of Liege, 4000 Liège, Belgium; nathalie.fagel@liege.be

<sup>7</sup> Géosciences Environnement Toulouse, UMR 5563, Université de Toulouse, CNRS-IRD-OMP-CNES, 31000 Toulouse, France; luc.bourrel@ird.fr

<sup>8</sup> INRAE, Bordeaux Sciences Agro, UMR 1391 ISPA, 33140 Villenave-d'Ornon, France; frederic.frappart@inrae.fr

<sup>9</sup> Facultad de Ciencias Ambientales, Universidad de Concepción, Concepcion 4030000, Chile; rurrutia@udec.cl

\* Correspondence: lien.rodriguez@uss.cl; Tel.: +56-999168115



**Citation:** Rodríguez-López, L.; Alvarez, D.; Bustos Usta, D.; Duran-Llacer, I.; Bravo Alvarez, L.; Fagel, N.; Bourrel, L.; Frappart, F.; Urrutia, R. Chlorophyll-a Detection Algorithms at Different Depths Using In Situ, Meteorological, and Remote Sensing Data in a Chilean Lake. *Remote Sens.* **2024**, *16*, 647. <https://doi.org/10.3390/rs16040647>

Academic Editor: Mhd. Suhby Salama

Received: 17 December 2023

Revised: 23 January 2024

Accepted: 5 February 2024

Published: 9 February 2024



**Copyright:** © 2024 by the authors. Licensee MDPI, Basel, Switzerland. This article is an open access article distributed under the terms and conditions of the Creative Commons Attribution (CC BY) license (<https://creativecommons.org/licenses/by/4.0/>).

**Abstract:** In this study, we employ in situ, meteorological, and remote sensing data to estimate chlorophyll-a concentration at different depths in a South American freshwater ecosystem, focusing specifically on a lake in southern Chile known as Lake Maihue. For our analysis, we explored four different scenarios using three deep learning and traditional statistical models. These scenarios involved using field data (Scenario 1), meteorological variables (Scenario 2), and satellite data (Scenarios 3.1 and 3.2) to predict chlorophyll-a levels in Lake Maihue at three different depths (0, 15, and 30 m). Our choice of models included SARIMAX, DGLM, and LSTM, all of which showed promising statistical performance in predicting chlorophyll-a concentrations in this lake. Validation metrics for these models indicated their effectiveness in predicting chlorophyll levels, which serve as valuable indicators of the presence of algae in the water body. The coefficient of determination values ranged from 0.30 to 0.98, with the DGLM model showing the most favorable statistics in all scenarios tested. It is worth noting that the LSTM model yielded comparatively lower metrics, mainly due to the limitations of the available training data. The models employed, which use traditional statistical and machine learning models and meteorological and remote sensing data, have great potential for application in lakes in Chile and the rest of the world with similar characteristics. In addition, these results constitute a fundamental resource for decision-makers involved in the protection and conservation of water resource quality.

**Keywords:** remote sensing; machine learning; lake; chlorophyll-a at depth

## 1. Introduction

Remote lakes, defined as bodies of water located in geographically isolated or inaccessible areas [1], are typically found in mountainous regions, polar landscapes, tropical rainforests, or anywhere with significant natural barriers, such as steep terrain or dense vegetation [2,3]. Their defining characteristics include their remoteness from urbanized areas and limited exposure to human activity [4]. The difficult accessibility of these lakes

often results in their preservation, allowing them to remain virtually untouched and to maintain their natural beauty and biodiversity [4–6]. Not having suffered direct human influence, these bodies of water offer pristine environments and relatively intact ecosystems [7,8]. In Chile, the Andes Mountains are home to numerous remote lakes due to the geomorphological characteristics of the country [9].

Due to their isolation and relative inaccessibility, remote lakes often become the focus of scientific studies and research aimed at understanding aquatic ecosystems and their interactions with the surrounding environment [10,11]. In addition, these lakes can play a crucial role in biodiversity conservation by acting as refuges for vulnerable or endangered species [12]. However, recent studies, including [13–15], have reported algal bloom episodes in mountain lakes away from humans and other settlements [14–16], where human influence is more pronounced.

With the development of technology and communications, remote sensing has become an alternative tool to traditional monitoring, especially in remote areas, such as lakes, where it provides valuable information on water quality parameters [17]. Chlorophyll-a is a pigment found in all aquatic and terrestrial plants and is an important indicator of water quality and the health of aquatic ecosystems [18]. Reflectance derived from bands of the electromagnetic spectrum can be obtained from multispectral images taken by various instruments aboard satellites [19,20]. Algorithms applied to these images use this information to extract relevant features from the images, such as the wavelength and intensity of reflected light, which are related to the presence of chlorophyll-a [21,22]. These features are combined with the data from the satellite and with training data from the machine learning model to create an algorithm that can detect and quantify chlorophyll-a in new images [23].

Chlorophyll-a detection algorithms using combined machine learning and remote sensing techniques are new advanced tools used to assess the presence and concentration of chlorophyll-a in water bodies [24–26]. Machine learning consists of training a model with previously labeled sample data, which allows the algorithm to learn to recognize patterns and make accurate predictions about chlorophyll-a concentration in new images [27–29]. The combination of machine learning and remote sensing techniques allows for improved accuracy of chlorophyll-a detection compared to traditional approaches [30–33]. These algorithms can be applied to different types of water bodies, such as lakes, rivers, and oceans, and are especially useful for large-scale water quality monitoring [34–37]. Accurate chlorophyll-a detection provides valuable information for water resource management, environmental impact assessments, and early detection of phenomena such as harmful algal blooms [38,39]. The objective of this work is to combine the previously described techniques of remote sensing and machine learning in a remote lake of the Andes Mountain range in Chile to predict the behavior of the variable chlorophyll-a concentrations at different depths as a bioindicator of the trophic state of this lake body. The specific objectives are as follows: (i) to collect baseline information on the behavior of limnological parameters in the period of 2001–2020; (ii) to create an estimation model of Chl-a using in situ, meteorological, and remote sensing data; and (iii) to validate the accuracy of the model with statistical metrics.

## 2. Materials and Methods

### 2.1. Site Description

Lake Maihue is located between 40°16'S and 72°03'W in the Los Rios region of southern Chile [40]. Maihue is an overdeepened glacial lake dammed by frontal moraines [41]. This lake in the Araucanian Lake District has a maximum depth of 207 m and covers an area of 47.2 km<sup>2</sup> [42]. Its waters are of an intense blue color and are fed by several rivers and streams that descend from the surrounding mountains [43]. In addition, Lake Maihue has several islands scattered across its surface, which adds visual appeal to its landscape. In terms of its geographic setting, Lake Maihue is in an area of abundant vegetation and native forests [43]. Native forests surround its shores, mainly of species such as *Nothofagus dombeyi* (coigüe), *Eucryphia cordifolia* (ulmo), and *Podocarpus nubigenus* (mañío). In addition,

nearby you can find waterfalls, rivers, and streams that are fed by melting glaciers in the Cordillera. The climate of the Andes is extreme, with strong winds, rainfall, and high solar radiation [44]. Lake Maihue has temperatures ranging from 6.5 °C in winter to 19.5 °C in summer (DGA Chile, accessed 28 June 2023).

## 2.2. Sampling Measurements and Meteorological Data

The Dirección General de Aguas de Chile (DGA) monitors several lakes in the Chilean territory, including Lake Maihue. For this study, we selected the monitoring campaigns carried out in the summer and spring from 2001 to 2020. The physicochemical and biological parameters of the water included in the chlorophyll-a estimation model were Chl-a, a Secchi disk, temperature (°C), total nitrogen (NT) (mg/L), total phosphorus (mg/L), and NTU turbidity. On the other hand, some meteorological variables, such as precipitation (mm), air temperature (°C), relative humidity (%), and wind speed (m/s), were selected. Precipitation was obtained from the Lago Maihue station (Figure 1) from the Dirección General de Aguas de Chile (DGA) at <https://dga.mop.gob.cl/Paginas/default.aspx> and consulted on 20 September 2023. This station is the closest and most representative of the lake.

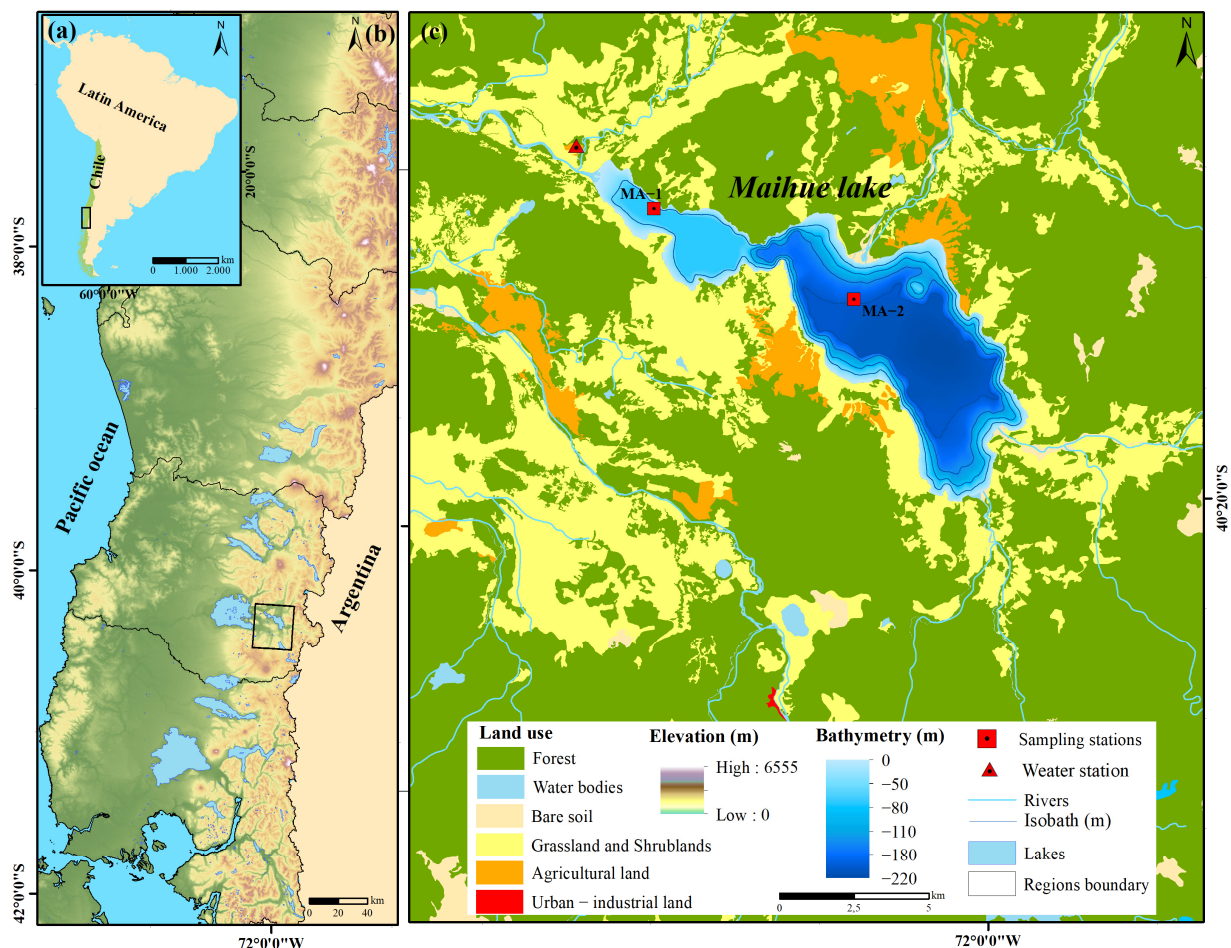


**Figure 1.** (a) Latin America continent; (b) region de Los Rios in Chile; (c) sampling stations at Lake Maihue, MA-1 (LOS LOLLLES) and MA-2 (CENTRO).

## 2.3. Satellite Images and Processing

The multispectral bands of the Landsat satellite have a high resolution of 30 m and cover the study period (2001–2020), which is why they were used in this research. Landsat is a project operated by the National Aeronautics and Space Administration (NASA) and the United States Geological Survey (USGS) [45], and images are available on the USGS Earth Explorer at <https://earthexplorer.usgs.gov/> accessed on 20 September 2023. A total

of 19 Landsat 5, 7, and 8 images (L-5, L-7, and L-8) were downloaded with a low percentage of clouds covering the study lake (path/row: 232/88 and 233/88) and corresponding to Collection 2 Level 1 (see Table 1). To mask clouds, quality assessment (QA) bands were used and analyzed by visual inspection. Only those with the lowest percentage of cloud cover over the lake and those as close as possible to the sampling dates were selected.

**Table 1.** Characteristics of satellite images.

| N  | Image Id                                 | Path/Row | Year | In Situ Date  | Image Date | Days Difference |
|----|--|----------|------|---------------|------------|-----------------|
| 1  | LE07_L1TP_233088_20020305_20211023_02_T1 | 233/88   | 2002 | 06-03-2002    | 05-03-2002 | 1               |
| 2  | LE07_L1TP_233088_20030324_20200915_02_T1 | 233/88   | 2003 | 18-03-2003    | 24-03-2003 | 6               |
| 3  | LT05_L1TP_233088_20031127_20201008_02_T1 | 233/88   | 2003 | 17-11-2003    | 27-11-2003 | 10              |
| 4  | LT05_L1TP_232088_20040311_20200903_02_T1 | 232/88   | 2004 | 01-03-2004    | 11-03-2004 | 10              |
| 5  | LT05_L1TP_232088_20040818_20200903_02_T1 | 232/88   | 2004 | 20-08-2004    | 18-08-2004 | 2               |
| 6  | LT05_L1TP_232088_20041122_20200902_02_T1 | 232/88   | 2004 | 17-11-2004    | 22-11-2004 | 5               |
| 7  | LT05_L1TP_232088_20060213_20200901_02_T1 | 232/88   | 2006 | 09-02-2006    | 13-02-2006 | 4               |
| 8  | LT05_L1TP_233088_20060527_20200901_02_T1 | 233/88   | 2006 | 24-05-2006    | 27-05-2006 | 3               |
| 9  | LT05_L1TP_233088_20060730_20200831_02_T1 | 233/88   | 2006 | 12-08-2006    | 30-07-2006 | 12              |
| 10 | LT05_L1TP_233088_20061103_20200831_02_T1 | 233/88   | 2006 | 26-10-2006    | 03-11-2006 | 7               |
| 11 | LT05_L1TP_233088_20070818_20200830_02_T1 | 233/88   | 2007 | 19-08-2007    | 18-08-2007 | 1               |
| 12 | LT05_L1TP_232088_20080219_20200829_02_T1 | 232/88   | 2008 | 23-02-2008    | 19-02-2008 | 4               |
| 13 | LT05_L1TP_232088_20090221_20200828_02_T1 | 232/88   | 2009 | 17-02-2009    | 21-02-2009 | 4               |
| 14 | LT05_L1TP_233088_20091111_20200825_02_T1 | 233/88   | 2009 | 17-11-2009    | 11-11-2009 | 6               |
| 15 | LC08_L1TP_233088_20131208_20200912_02_T1 | 233/88   | 2013 | 03/05-12-2013 | 08-12-2013 | 3, 5            |
| 16 | LC08_L1TP_233088_20140226_20200911_02_T1 | 233/88   | 2014 | 19-02-2014    | 26-02-2014 | 7               |
| 17 | LC08_L1TP_233088_20150213_20200909_02_T1 | 233/88   | 2015 | 10/11-02-2015 | 13-02-2015 | 2, 3            |
| 18 | LC08_L1TP_233088_20200126_20200823_02_T1 | 233/88   | 2020 | 26-01-2020    | 26-01-2020 | 0               |
| 19 | LC08_L1TP_232088_20201118_20210315_02_T1 | 232/88   | 2020 | 22-11-2020    | 18-11-2020 | 4               |

Images were atmospherically corrected in the ACOLITE software (version 20211124.0) at <https://github.com/acolite> accessed on 20 September 2023. This software contains the atmospheric correction protocols and processing developed at RBINS for aquatic remote sensing applications (Ilori et al., 2019). The default atmospheric correction used was the DSF algorithm approach “Dark Spectrum Fitting” [46–48] and the older “exponential extrapolation” or EXP algorithm [49–51]. From the processing, surface-level reflectance ( $\rho_s$ ) is obtained, and the values are extracted per  $3 \times 3$  pixel matrix [15,52]. The software used to extract the pixel values was ArcGIS (ESRI v. 10.8.2). Then, the values of the band combinations and the calculated spectral indices are also obtained. The area of interest (Roi) was established from geospatial data provided by the General Directorate of Waters of Chile (DGA), accessed on 02 March 2023.

#### 2.4. Vegetation Indices, Band, and Band Combination

Water quality parameters, such as chlorophyll, have been estimated with great precision using satellite data in lakes [18,39,53,54]. The blue (B), green (G), red (R), near infrared (NIR), and shortwave infrared (SWIR) multispectral bands were used, as well as some combinations of bands and vegetation spectral indices (see Table 2). The spectral bands and their combinations (N/R, R/N, and B/G) have been widely used in the literature due to their excellent results in retrieving the concentration of chlorophyll [18,39,55,56]. Furthermore, spectral indices derived from the above-mentioned bands are currently the most used ones for monitoring the concentration of chlorophyll [14,39,57,58]. The normalized difference vegetation index (NDVI), obtained as the ratio between the NIR and R reflectances and their sum, is an indicator of photosynthetic activity and changes in vegetation [59,60]. The surface algal bloom index (SABI), obtained as the ratio between the NIR and R reflectances

and the sum of the B and G reflectances, is an index proposed to delineate the spatial distributions of floating algae or emergent vegetation extraction in aquatic systems [15,61]. The floating algal index (FAI) is an indicator capable of detecting floating algae in different aquatic environments and is a very efficient index for the detection of surface vegetation related to chlorophyll. It is obtained from the relationships between the NIR, R, and SWIR bands [62,63]. The green normalized difference vegetation index (GNDVI) is resistant to atmospheric effects and very sensitive to chlorophyll-a concentrations. It is calculated from the NIR and G bands [55,64]. The last index calculated was the green chlorophyll index (GCI) [65,66]. This can be used to estimate the chlorophyll content of leaves and has been used to detect chlorophyll and algal blooms in some research. It uses NIR and G wavelengths [15].

**Table 2.** Definition of the spectral indices used in this study.

| Indices  | Formula   | Reference |
|--|---|-----------|
| Spectral bands                                       | 4 bands (B, R, G, NIR)  | [18]      |
| Floating Algal Index (Fai)                           | $FAI = R_{nir} - R'_{nir}$<br>$R'_{nir} = R_{red} + (R_{swir} - R_{red}) \times (\lambda_{nir} - \lambda_{red}) / (\lambda_{swir} - \lambda_{red})$ | [40]      |
| Green Normalized Difference Vegetation Index (Gndvi) | $(NIR - G) / (NIR + G)$   | [13]      |
| Normalized Difference Vegetation Index (Ndvi)        | $(NIR - R) / (NIR + R)$   | [13]      |
| Surface Algal Bloom Index (Sabi)                     | $(NIR - R) / (B + G)$   | [15]      |
| Green Chlorophyll Index (Gci)                        | $GCI = (NIR/G) - 1$   | [13]      |

## 2.5. Prediction Using Statistical and Machine Learning Models

### 2.5.1. SARIMAX

The SARIMAX (seasonal autoregressive integrated moving average with exogenous regressors) model is an extension of the SARIMA (seasonal autoregressive integrated moving average) model that allows for the inclusion of exogenous variables in time series modeling (see Figure 2). SARIMA models are used to analyze and predict time series, which are sequences of observed data at regular time intervals.

The mathematical model is defined by Equation (1):

$$y_t = \beta_t x_t + u_t$$

$$\varphi_p(L)\tilde{\varphi}_p(L^s)\Delta^d\Delta_s^D u_t = A(t) + \theta_q(L)\tilde{\theta}_q(L^s)\zeta \quad (1)$$

where  $\beta$  in the first part of the formula represents external variables. The model is similar to the SARIMA model, with the following hyperparameters [67]:

p represents the order for the autoregressive part (AR);

q represents the order for the moving average part (MA);

I represent the differencing order;

P represents the seasonal AR order;

Q represents the seasonal MA order;

D represents the seasonal differencing;

s = 12, 24 represents the seasonal coefficients.

The general fit procedure involves computing ACF and PACF, then applying the Dickey Fuller test to evaluate stationarity. Additionally, we introduce necessary seasonal or order differences to determine the optimal hyperparameters, as outlined by [14].

In the SARIMAX model, the process starts with the time series dataset; therefore, the SARIMAX model could include a seasonal component alongside exogenous variables. Afterwards, several preprocessing steps are implemented (differentiation, scaling, and outliers' removal) alongside parameter estimation using Akaike Information Criteria (AIC)

and Bayesian Information Criteria (BIC) to select the best model. Finally, the trained model is used to forecast new values [68].

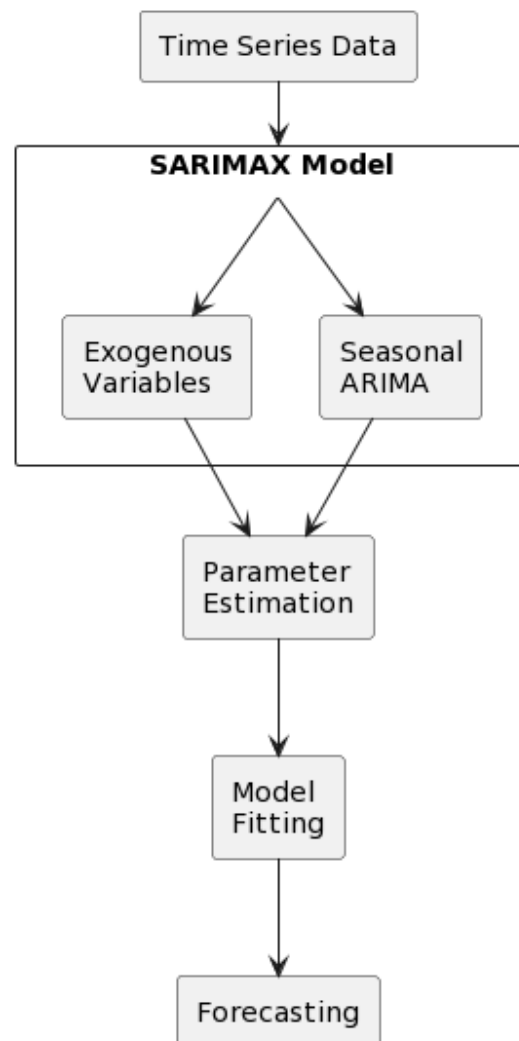


**Figure 2.** SARIMAX architecture.

### 2.5.2. DGLM

The Dynamic Generalized Linear Model (DGLM) is an approach based on the prior and posteriori distributions of the data (see Figure 3). If we have a simple model for every timestamp,  $t$  is defined as follows:

$$p(Y_t | \eta_t, \phi) = \exp\{\phi\{Y_t \eta_t - a(\eta_t)\}\} b(Y_t, \phi) \quad (2)$$

where

$Y_t$  is the random variable at time  $t$ ;

$a(\eta_t)$  is a function of the parameters to adjust the shape of the random variable distribution;

$b(Y_t, \phi)$  represent a normalizing function that ensures the probability distribution integrates (or sums) to 1;

$\eta_t$  is the natural parameter of the distribution satisfying the following:

$$E[Y_t | \eta_t, \phi] = \mu_t = a'(\eta_t) \quad (3)$$

and  $\phi$  is a scale parameter with the following:

$$V[Y_t | \eta_t, \phi] = \ddot{a}(\eta_t) / \phi \quad (4)$$

We also define a conjugate prior for  $\eta_t$  named  $CP[a_t, \beta_t]$ . Therefore, a dynamic extension of the standard generalized linear model (GLM) can be defined relating  $\eta_t$  to the nonlinear transformation  $g(\eta_t)$ , where  $g(\cdot)$  is a link function for simple linear regression given by  $g(\eta_t) = \eta_t$ , with the following structure:

$$\lambda_t = F_t' \theta_t \quad (5)$$

where

$\lambda_t$  represents the mean of the response variable;

$F_t$  is a design matrix or set of features associated with observations;

$\theta_t$  is an underlying state vector having a time evolution similar to that of the DLM. All the mathematical derivations for this model are described by [69].

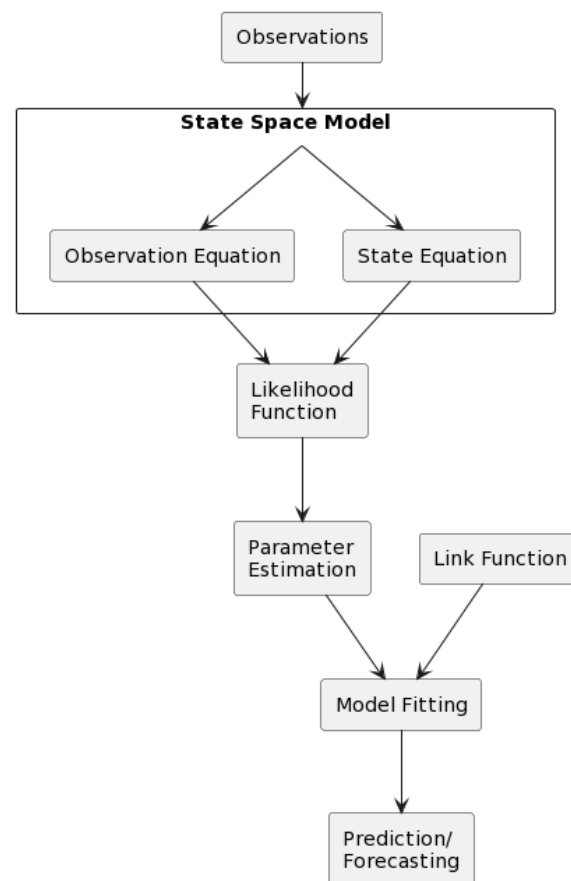


**Figure 3.** DGLM architecture.

The DLGM model starts receiving time series data observations. Subsequently, the construction of a state space model delineates the temporal evolution of the system based on its underlying state. Following this, the likelihood function assesses the probability of data observation given specific assumptions (conditional probability). Parameter estimation is then undertaken, while the link function specifies the association between the predictors and the response variable. Afterwards, refinement of the learning process is accomplished through model fitting with the data, facilitating the precise representation of relationships. Ultimately, the dynamic model enables accurate forecasting across diverse contexts [69].

### 2.5.3. LSTM

Long short-term memory (LSTM) is a variant of a recurrent neural network (RNN) proposed by Hochreiter and Schmidhuber in 1997 [70]. This algorithm solves the long-term dependency problem in RNNs by introducing memory (C) and an appropriate gate structure.

The LSTM cell (Figure 2) has four gates: input (*i*), forget (*f*), control (*c*), and output gates (*o*). The input gate determines the information that can be inserted and transferred to the cell:

$$i_t = \sigma(W_i \cdot [h_{t-1}, x_t] + b_i) \quad (6)$$

The forget gate decides which information from the input is important from previous memory as follows:

$$f_t = \sigma(W_f \cdot [h_{t-1}, x_t] + b_f) \quad (7)$$

The control gate stabilizes the update in the cell state from  $C_{t-1}$  to  $C_t$  using Equations (8) and (9):

$$\tilde{C}_t = \tanh(W_c \cdot [h_{t-1}, x_t] + b_c) \quad (8)$$

$$C_t = f_t \times C_{t-1} + \tilde{C}_t \quad (9)$$

Additionally, the output gate generates the output, updating the hidden vector  $h_{t-1}$  with Equations (10) and (11):

$$o_t = \sigma_t \times \tanh(C_t) \quad (10)$$

$$h_t = o_t \times \tanh(C_t) \quad (11)$$

where  $\sigma$  is the activation function,  $W$  corresponds to the weight matrices calibrated during the training process,  $\tanh$  is used to scale values in the range of  $-1$  to  $1$ , and  $b$  represents the bias in each step. During the training process, the lags ranging from 9 to 15 and the number of cells ranging from 30 to 50 were evaluated to identify the best-performing hyperparameter configuration based on the size and complexity of each dataset. Furthermore, a dense layer is employed as the output layer to facilitate accurate predictions. The latter topology is a common configuration in the LSTM algorithm [71].

To test the prediction's performance and relative importance, the different scenarios (1, 2, and 3) are defined as follows:

- Scenario 1 (measurement data): in the first case, we include the actual variables measured during the monitoring campaigns for the four seasons of the year and in the two seasons of the lake (Chl-a, SD, Temp, NT, Pt, and NTU).
- Scenario 2 (meteorological variables): in addition to the actual variables, we include meteorological variables as conditioning variables that can influence the autochthonous processes of the lake (precipitation, air temperature, relative humidity, and wind speed).
- Scenario 3 (satellite data): In this case, we include a sub-case of spectral bands from Landsat satellite processing and another sub-case including vegetation spectral indices.

### 2.6. Statistics Validation

In Section 2.6, we evaluate the performance of the defined models using several metrics. These metrics include the mean squared error (MSE), as detailed in [72], the root mean squared error (RMSE), as explained in [18], the mean absolute error (MAE), the maximum error, as described in [73], and  $R^2$ , following an approach like the one presented in [14]. These metrics provide information on the accuracy, precision, and potential limitations of the chlorophyll-a estimation.

The dataset was divided into training and test datasets, with details provided in Table 3. A sequential splitting method was employed, following the 70/30% rule, to calculate the various error metrics. In this approach, the time series data were divided into



two segments: the first part was used for model training, while the latter was used for model validation. This strategy was applied to different monitoring stations (see Figure 1) and has been shown to provide good performance for evaluating the performance of deep learning models in time series analysis [74,75].

**Table 3.** Training and test datasets used in the statistical and machine learning models.

| Station/Depth | 0 M (Train/Test) | 15 M (Train/Test) | 30 M (Train/Test) |
|---------------|------------------|-------------------|-------------------|
| CENTRO        | 38/16            | 38/16             | 38/16             |
| LOS LOLLES    | 28/12            | 28/12             | 28/12             |

### 3. Results

#### 3.1. Behavior of Chl-a, SD, and T Values at Depth

Figure 4 shows the behavior of limnological parameters during the study period (2001–2020) at different depths for two stations of Lake Maihue during the four seasons of the year. The Chl-a values range from a maximum of 3.10 ( $\mu\text{g/L}$ ) in the summer season and a maximum of 2.59 in the spring since these seasons are the most productive due to their seasonal characteristics, where there is a higher water temperature and hydrodynamic stability of the lake, to minimum values of 0.2 ( $\mu\text{g/L}$ ) in the winter. Transparency varies between maximums of 19.5 m according to the Secchi disk in the summer due to the great penetration of solar radiation at depth and minimum values of 2.30 m in winter and autumn due to the mixing present in the lake by rainfall, strong winds, and the turbidity generated by these conditions in the water. The minimum temperature is 7.96 degrees in the winter, and in the summer, it reaches 21.98 degrees, which is quite high for these latitudes, a possible effect of the increases attributed to the surface temperature in lakes due to the current climate crisis. Figure 5 shows the spatial behavior of Chl-a at different depths. For more details of the limnological parameters, see Tables S1–S4.

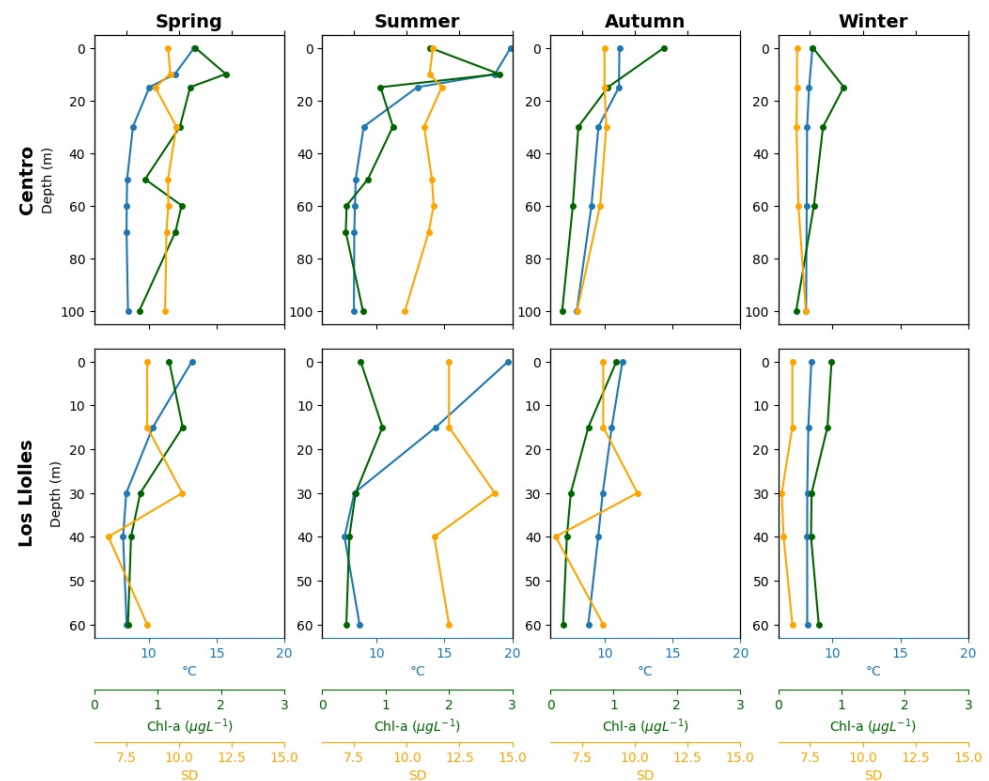


**Figure 4.** Seasonal behavior of limnological parameters (Chl-a, SD, and T) based on the mean observed state from 2001 to 2020 at two stations at different depths in Lake Maihue.

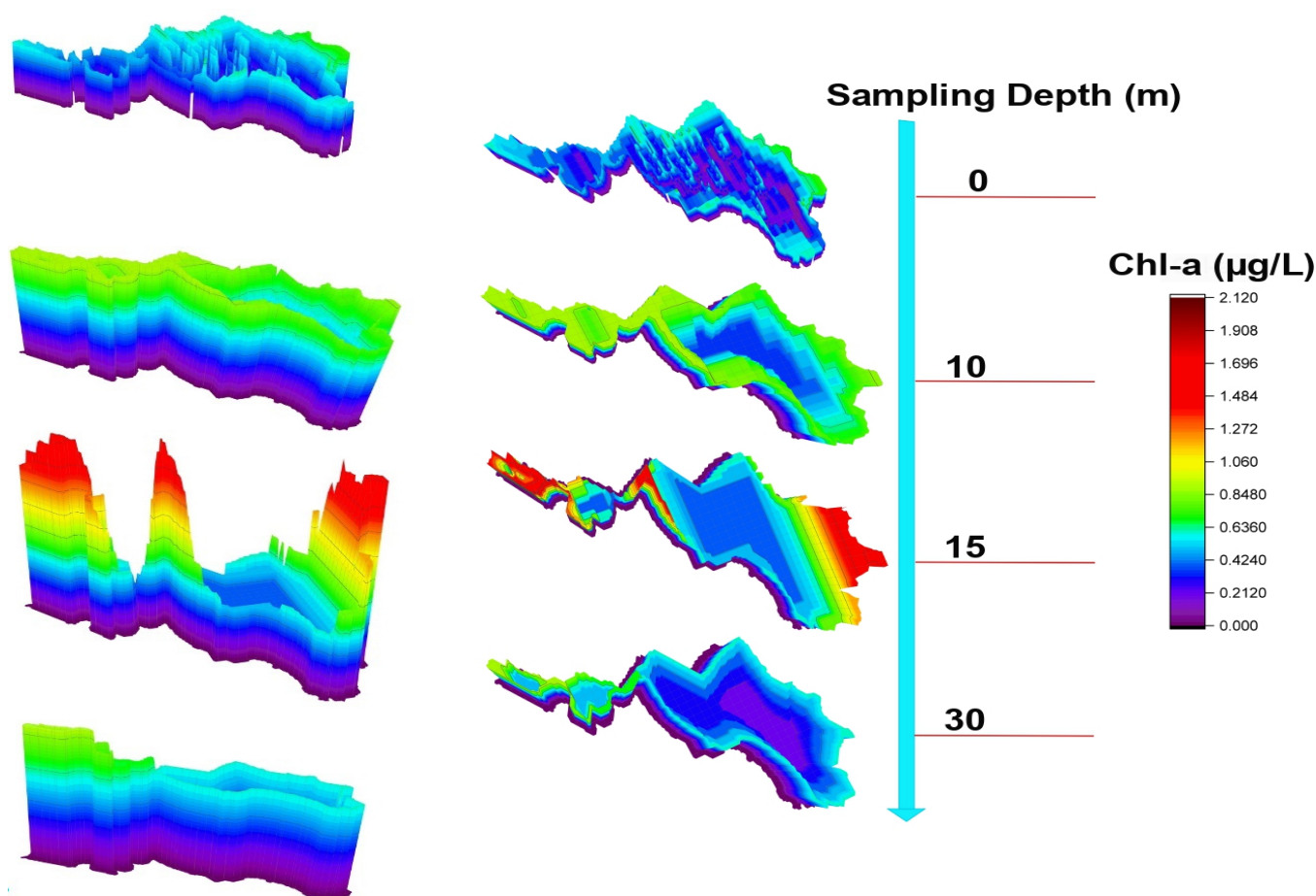


**Figure 5.** Concentration of Chl-a in a 3D model of Lake Maihue at different depths during the summer season.

### 3.2. Important Features

Figure 6 shows, using the Garson weighting method [76], the relative importance or contribution of the independent variables (predictor variables) in explaining the variance of the dependent variable (result variable) for each of the cases used.

The results showed that total nitrogen (NT), total phosphorus (Pt), and turbidity (NTU) present the highest values of relative importance (ranging between 0.20 and 0.29) in the prediction of chlorophyll-a in the two stations of Case 1. Subsequently, air temperature (Air. Temp) and wind (Wind) showed relative importance, ranging between 0.28 and 0.31, with wind being more significant than air temperature. On the contrary, transparency (SD), relative humidity (Real.Hum), and precipitation (Precip) show relatively minor importance, with all values lower than 0.20.

In the last two scenarios, where the satellite bands were used independently (Scenario 3.1) and the vegetation indices (Scenario 3.2), they showed a high importance in the prediction of Chl-a, with values higher than 0.18 in all cases. The independent bands green (G) and red (red) proved to be the ones that best explain the behavior of the variable for Lake Maihue, with values above 0.28 in all cases.

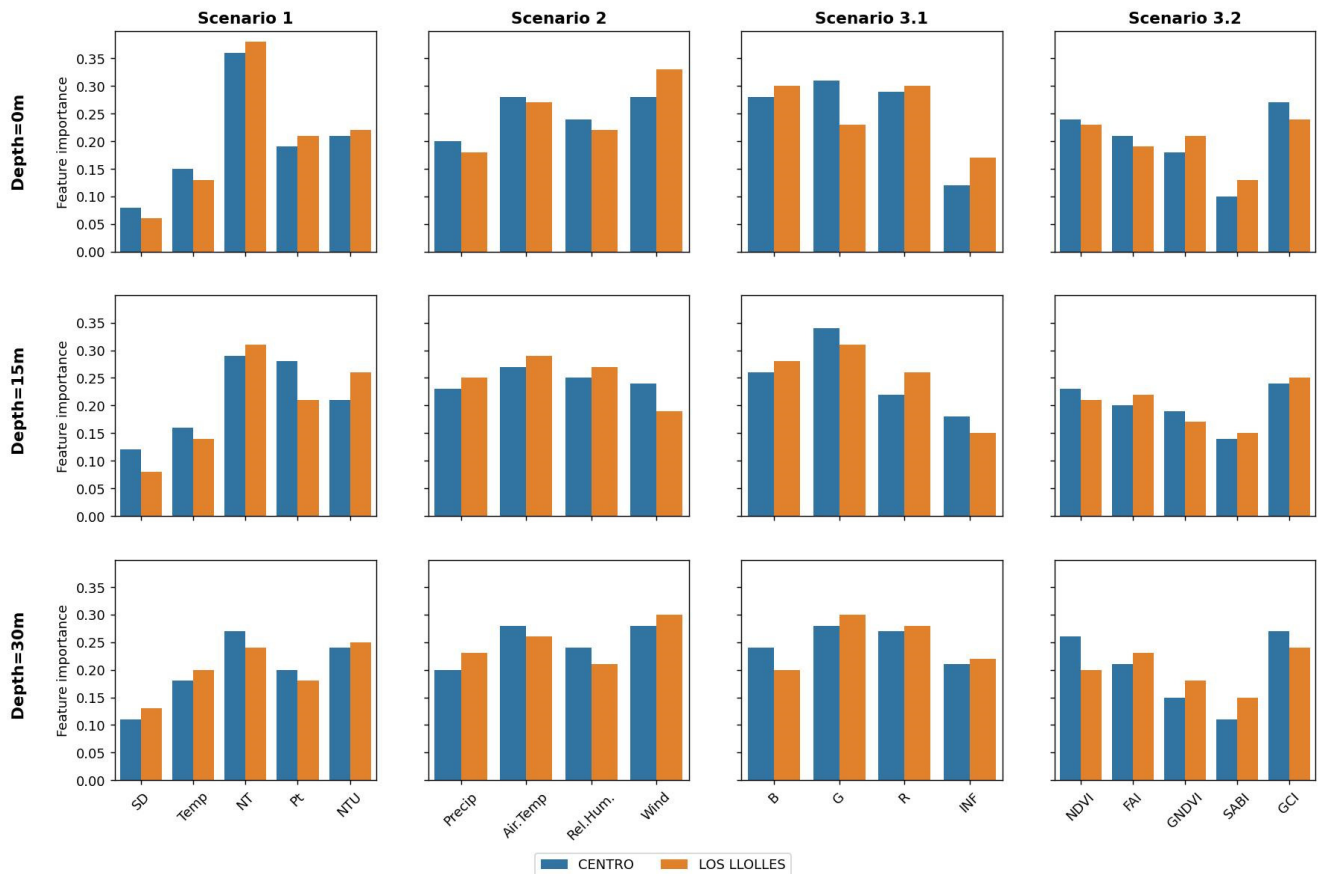


**Figure 6.** Relative importance using Garson’s weighting method for all scenarios for two sampling stations. In Scenario 1, SD is Secchi disk, Temp is temperature of the water, NT is total nitrogen, Pt is total phosphorous, and NTU is turbidity. In Scenario 2, Precip is precipitation, Air.Temp is temperature of the air, Real.Hum is relative humidity, and Wind is wind. In Scenario 3.1, B is blue band, G is green band, R is red band, and INF is infrared band. Finally, in Scenario 3.3, NDVI is normalized difference vegetation index, FAI is flotation algal index, GNDVI is green normalized difference index, SABI is surface algal bloom index, and GCI is green chlorophyll index.

### 3.3. Chl-a Estimation Scenarios

#### Scenario 1. In situ variables (Chl-a, SD, Temp, NT, Pt, NTU)

The temporal variations in the concentration of chlorophyll measured in situ and derived from statistical and machine learning techniques at different depths (0 m, 15 m, and 30 m) and for two stations (CENTRO and LOS LLOLLES) are presented in Figure 7. The performances of these methods using the metrics described in Section 2.6 are presented in Table 4. SARIMAX and LSTM exhibit a broader dispersion range, with MSE values spanning from 0.30 to 0.90 and 0.19 to 0.82, respectively, across all depths and stations. Conversely, DLGM demonstrates a lower spread, with MSE values ranging from 0.24 to 0.72, with very good performance at 15 m depth. It is noteworthy that the most significant performance deficit for the CENTRO (LOS LLOLLES) station is observed at 0 (30) m depth, characterized by elevated MSE, RMSE, max error, and MAE metrics.

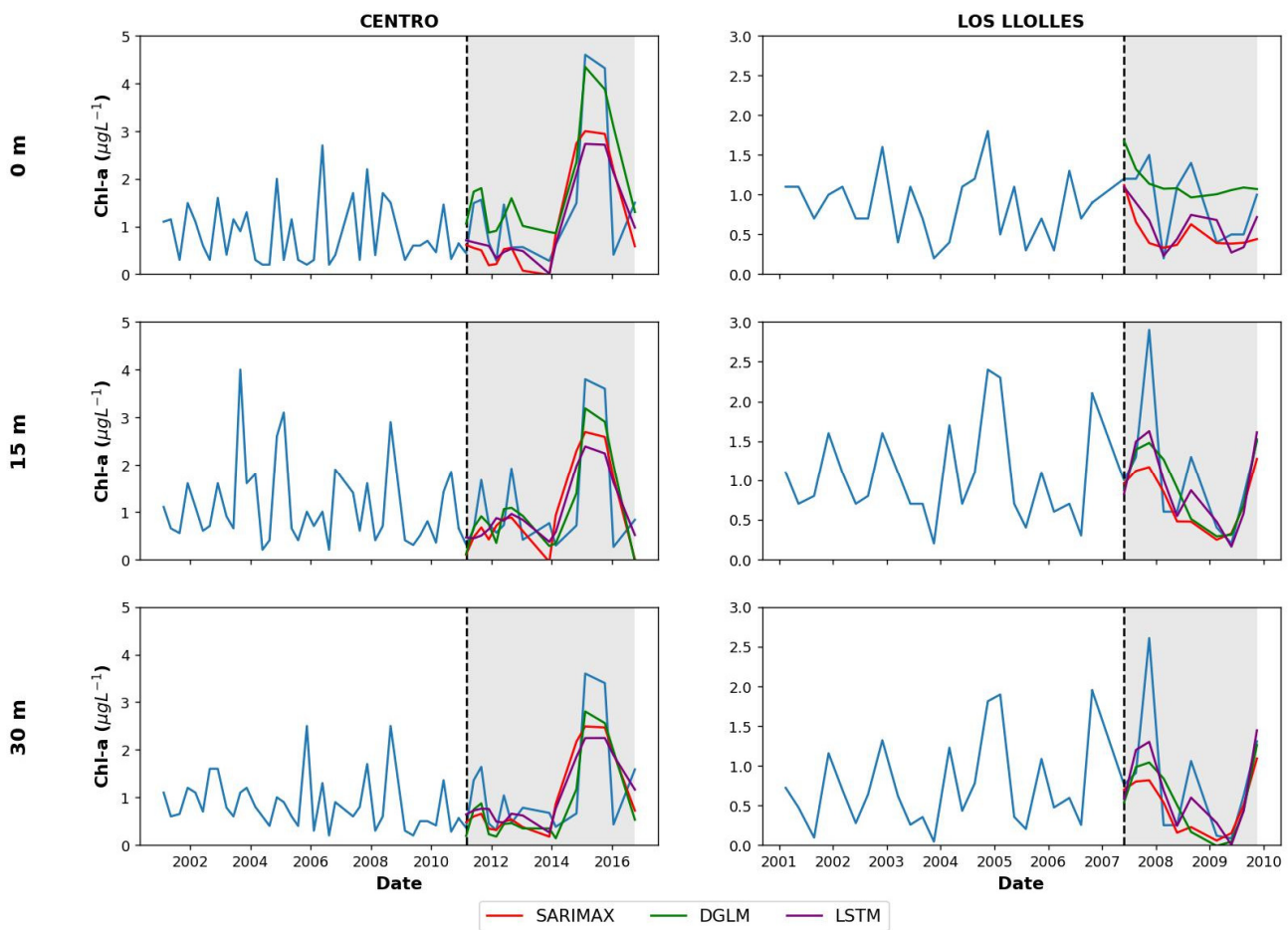


**Figure 7.** Chlorophyll-a estimation for Scenario 1 in the two sampling stations with data from Maihue Lake during 2001–2016. The shaded regions represent observations for the selection of the test. The blue line represents the in situ data.

**Table 4.** Validation metrics for all the stations and models considered in Scenario 1.

| Model/Station | Station     | Depth | MSE<br>( $\mu\text{g/L}$ ) <sup>2</sup> | RMSE<br>( $\mu\text{g/L}$ ) | MaxError<br>( $\mu\text{g/L}$ ) | MAE<br>( $\mu\text{g/L}$ ) | R <sup>2</sup> |
|---------------|-------------|-------|---|-----------------------------|---------------------------------|----------------------------|----------------|
| SARIMAX       | CENTRO      | 0 m   | 0.90                                    | 0.95                        | 2.59                            | 0.94                       | 0.35           |
|               |             | 15 m  | 0.73                                    | 0.85                        | 2.38                            | 0.98                       | 0.34           |
|               |             | 30 m  | 0.66                                    | 0.81                        | 2.37                            | 0.92                       | 0.32           |
|               | LOS LLOLLES | 0 m   | 0.30                                    | 0.55                        | 1.11                            | 0.41                       | 0.30           |
|               |             | 15 m  | 0.39                                    | 0.62                        | 1.73                            | 0.38                       | 0.43           |
|               |             | 30 m  | 0.41                                    | 0.64                        | 1.79                            | 0.36                       | 0.35           |
| DGLM          | CENTRO      | 0 m   | 0.72                                    | 0.85                        | 2.68                            | 0.59                       | 0.57           |
|               |             | 15 m  | 0.47                                    | 0.69                        | 1.74                            | 0.54                       | 0.61           |
|               |             | 30 m  | 0.46                                    | 0.68                        | 1.55                            | 0.55                       | 0.58           |
|               | LOS LLOLLES | 0 m   | 0.24                                    | 0.49                        | 0.94                            | 0.42                       | 0.50           |
|               |             | 15 m  | 0.33                                    | 0.57                        | 1.42                            | 0.37                       | 0.47           |
|               |             | 30 m  | 0.43                                    | 0.66                        | 1.67                            | 0.45                       | 0.38           |
| LSTM          | CENTRO      | 0 m   | 0.82                                    | 0.91                        | 1.87                            | 0.66                       | 0.52           |
|               |             | 15 m  | 0.69                                    | 0.83                        | 1.41                            | 0.66                       | 0.43           |
|               |             | 30 m  | 0.60                                    | 0.77                        | 1.46                            | 0.63                       | 0.58           |
|               | LOS LLOLLES | 0 m   | 0.19                                    | 0.43                        | 0.82                            | 0.35                       | 0.37           |
|               |             | 15 m  | 0.21                                    | 0.46                        | 1.28                            | 0.29                       | 0.61           |
|               |             | 30 m  | 0.23                                    | 0.48                        | 1.30                            | 0.32                       | 0.65           |

Additionally,  $R^2$  values reveal diverse trends, spanning from 0.30 to 0.65, with DLGM and LSTM models exhibiting superior values compared to SARIMAX performance (Table 4). It is important to note that  $R^2$  is an estimator significantly influenced by outliers, as evidenced in this instance in the test data considered for the analysis. Consequently, it cannot be solely relied upon as an exclusive performance indicator.

Overall, LSTM and DLGM perform better than SARIMAX at the CENTRO station. Conversely, SARIMAX appears to be a viable alternative for the LOS LLOLLES station. However, the choice between them depends on specific depth and station requirements, with LSTM (DLGM) performing well at CENTRO (LOS LLOLLES), with better results at 15 m depth.

### Scenario 2. Meteorological variables (precipitation, air temperature, relative humidity, and wind speed)

Time variations in chlorophyll concentration measured in situ and obtained from statistical and machine learning techniques at different depths (0 m, 15 m, and 30 m) and for two stations (CENTRO and LOS LLOLLES) are presented in Figure 8. The performances of these methods using the statistical metrics described in Section 2.6 are presented in Table 5.

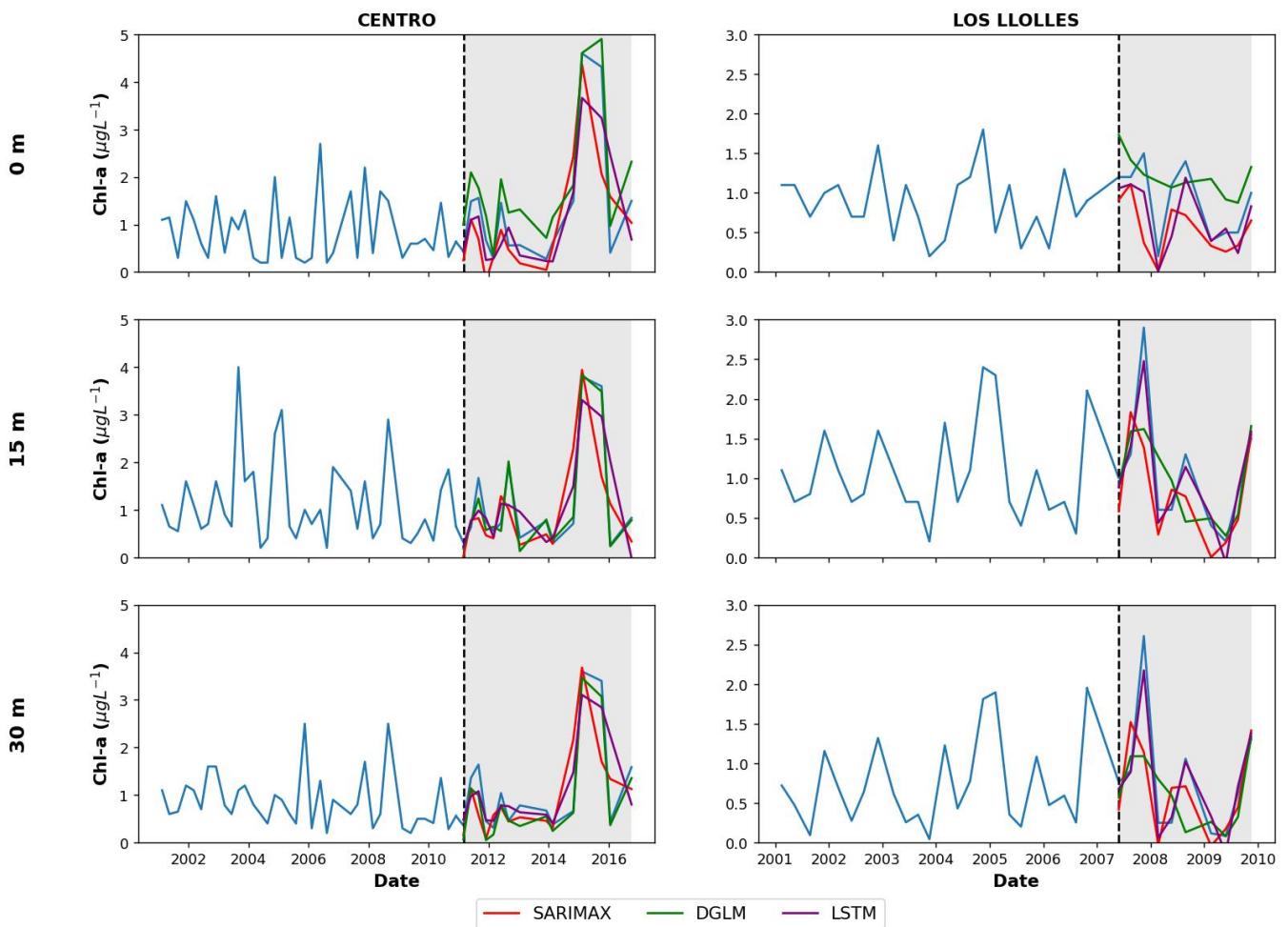


**Figure 8.** Chlorophyll-a estimation for Scenario 2 in the two sampling stations with data from Maihue Lake during 2001–2016. The shaded regions represent observations for the selection of the test.

The DLGM model performed very well at the CENTRO station, with  $R^2$  values between 0.84 and 0.93 and MSE values between 0.03 and 0.28, presenting a higher degree of correspondence at 15 m depth. Furthermore, LSTM excels as the most performant model at the LOS LLOLLES station, with notable lower MSE values compared to the other

two models, ranging from 0.03 to 0.09, and higher correlations (up to 0.94 at 30 m depth) (Table 5). Overall, LSTM exhibited better performance error metrics compared to SARIMAX (Table 5).

**Table 5.** Validation metrics for all the stations and models considered in Scenario 2.

| Model/Station | Station     | Depth | MSE ( $\mu\text{g/L}^2$ ) | RMSE ( $\mu\text{g/L}$ ) | MaxError ( $\mu\text{g/L}$ ) | MAE ( $\mu\text{g/L}$ ) | R <sup>2</sup> |
|---------------|-------------|-------|---------------------------|--------------------------|------------------------------|-------------------------|----------------|
| SARIMAX       | CENTRO      | 0 m   | 0.65                      | 0.81                     | 3.96                         | 0.93                    | 0.32           |
|               |             | 15 m  | 0.62                      | 0.79                     | 3.54                         | 0.96                    | 0.31           |
|               |             | 30 m  | 0.52                      | 0.72                     | 3.57                         | 0.88                    | 0.29           |
|               | LOS LLOLLES | 0 m   | 0.22                      | 0.47                     | 1.13                         | 0.35                    | 0.54           |
|               |             | 15 m  | 0.34                      | 0.59                     | 1.51                         | 0.43                    | 0.65           |
|               |             | 30 m  | 0.35                      | 0.59                     | 1.57                         | 0.42                    | 0.52           |
| DGLM          | CENTRO      | 0 m   | 0.28                      | 0.53                     | 0.82                         | 0.47                    | 0.84           |
|               |             | 15 m  | 0.03                      | 0.16                     | 0.43                         | 0.13                    | 0.98           |
|               |             | 30 m  | 0.08                      | 0.28                     | 0.64                         | 0.23                    | 0.93           |
|               | LOS LLOLLES | 0 m   | 0.24                      | 0.49                     | 0.94                         | 0.42                    | 0.50           |
|               |             | 15 m  | 0.32                      | 0.56                     | 1.28                         | 0.41                    | 0.43           |
|               |             | 30 m  | 0.42                      | 0.65                     | 1.62                         | 0.43                    | 0.46           |
| LSTM          | CENTRO      | 0 m   | 0.57                      | 0.76                     | 2.06                         | 0.55                    | 0.67           |
|               |             | 15 m  | 0.47                      | 0.68                     | 1.77                         | 0.53                    | 0.62           |
|               |             | 30 m  | 0.39                      | 0.62                     | 1.82                         | 0.43                    | 0.65           |
|               | LOS LLOLLES | 0 m   | 0.09                      | 0.29                     | 0.65                         | 0.22                    | 0.55           |
|               |             | 15 m  | 0.04                      | 0.19                     | 0.42                         | 0.16                    | 0.93           |
|               |             | 30 m  | 0.03                      | 0.19                     | 0.43                         | 0.14                    | 0.94           |

### Scenario 3. Satellite data:

#### 3.1 Spectral Bands (B, G, R, and INR).

Seasonal fluctuations in chlorophyll concentration, evaluated in situ and extrapolated using statistical and machine learning techniques at various depths (0 m, 15 m, and 30 m) and for two stations (CENTRO and LOS LLOLLES), are presented in Figure 9. The performance of these methods, evaluated based on the statistical metrics described in Section 2.6, is illustrated in Table 6. SARIMAX showed a good performance at the CENTRO station across all depths. DGLM presented slightly higher MSE values compared to SARIMAX, with lower RMSE values at 15 m depth. LSTM also showed good performance metrics, with MSE values ranging from 0.15 to 0.81; however, it did not perform well in the LOS LLOLLES station at 15 m.

**Table 6.** Validation metrics for all the stations and models considered in Scenario 3.1.

| Model/Station | Station     | Depth | MSE ( $\mu\text{g/L}^2$ ) | RMSE ( $\mu\text{g/L}$ ) | MaxError ( $\mu\text{g/L}$ ) | MAE ( $\mu\text{g/L}$ ) | R <sup>2</sup> |
|---------------|-------------|-------|---------------------------|--------------------------|------------------------------|-------------------------|----------------|
| SARIMAX       | CENTRO      | 0 m   | 0.60                      | 0.77                     | 3.20                         | 0.93                    | 0.33           |
|               |             | 15 m  | 0.47                      | 0.69                     | 2.81                         | 0.96                    | 0.30           |
|               |             | 30 m  | 0.39                      | 0.63                     | 2.88                         | 0.94                    | 0.29           |
|               | LOS LLOLLES | 0 m   | 0.19                      | 0.44                     | 0.86                         | 0.36                    | 0.38           |
|               |             | 15 m  | 0.22                      | 0.47                     | 1.34                         | 0.29                    | 0.58           |
|               |             | 30 m  | 0.43                      | 0.49                     | 1.33                         | 0.33                    | 0.54           |

Table 6. Cont.

| Model/Station | Station     | Depth | MSE ( $\mu\text{g/L}^2$ ) | RMSE ( $\mu\text{g/L}$ ) | MaxError ( $\mu\text{g/L}$ ) | MAE ( $\mu\text{g/L}$ ) | R <sup>2</sup> |
|---------------|-------------|-------|---------------------------|--------------------------|------------------------------|-------------------------|----------------|
| DGLM          | CENTRO      | 0 m   | 0.87                      | 0.93                     | 1.96                         | 0.75                    | 0.48           |
|               |             | 15 m  | 0.61                      | 0.78                     | 1.76                         | 0.55                    | 0.49           |
|               |             | 30 m  | 0.52                      | 0.73                     | 0.75                         | 0.53                    | 0.48           |
|               | LOS LLOLLES | 0 m   | 0.30                      | 0.55                     | 0.95                         | 0.46                    | 0.32           |
|               |             | 15 m  | 0.35                      | 0.59                     | 1.40                         | 0.39                    | 0.46           |
|               |             | 30 m  | 0.43                      | 0.66                     | 1.61                         | 0.42                    | 0.45           |
| LSTM          | CENTRO      | 0 m   | 0.81                      | 0.90                     | 1.94                         | 0.73                    | 0.52           |
|               |             | 15 m  | 0.73                      | 0.85                     | 1.84                         | 0.68                    | 0.39           |
|               |             | 30 m  | 0.63                      | 0.80                     | 1.75                         | 0.63                    | 0.38           |
|               | LOS LLOLLES | 0 m   | 0.15                      | 0.38                     | 1.04                         | 0.24                    | 0.42           |
|               |             | 15 m  | 0.29                      | 0.54                     | 1.41                         | 0.41                    | 0.44           |
|               |             | 30 m  | 0.28                      | 0.53                     | 1.33                         | 0.39                    | 0.56           |

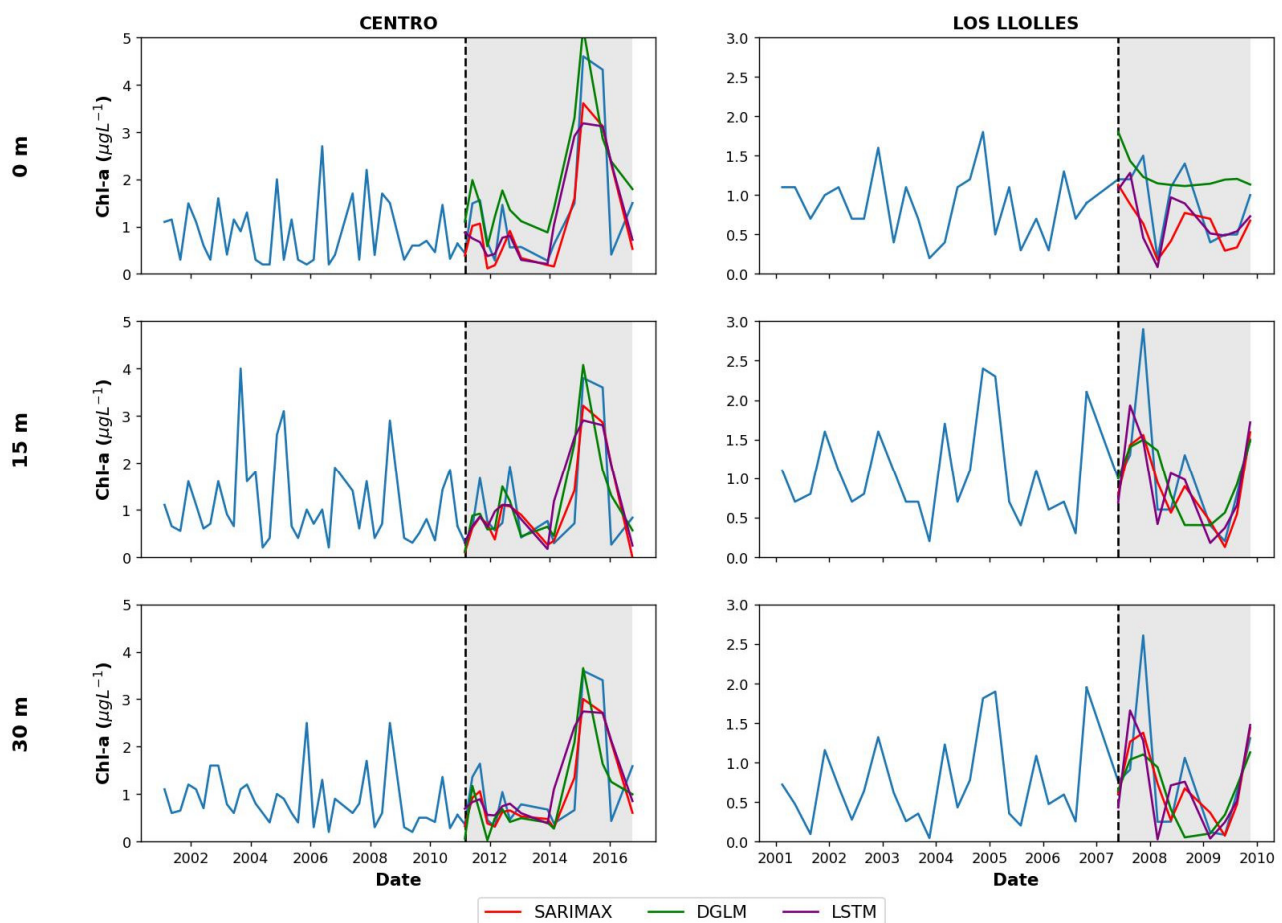


**Figure 9.** Chlorophyll-a estimation for Scenario 3.1 in the two sampling stations with data from Maihue Lake during 2001–2016. The shaded regions represent observations for the selection of the test.

### 3.2 Scenario 3.2. Vegetation Indices

Temporal fluctuations in chlorophyll concentration, evaluated in situ and extrapolated using statistical and machine learning techniques at various depths (0 m, 15 m, and 30 m) and for two stations (CENTRO and LOS LLOLLES), are presented in Figure 10. The effectiveness of these methods, evaluated based on the statistical metrics described in Section 2.6, is illustrated in Table 7. In general, a better performance can be observed at the

LOS LLOLLES station when compared to the performance at the CENTRO station. The best performance is observed at 15 m with SARIMAX, and the DGLM model showed the better performance metrics.

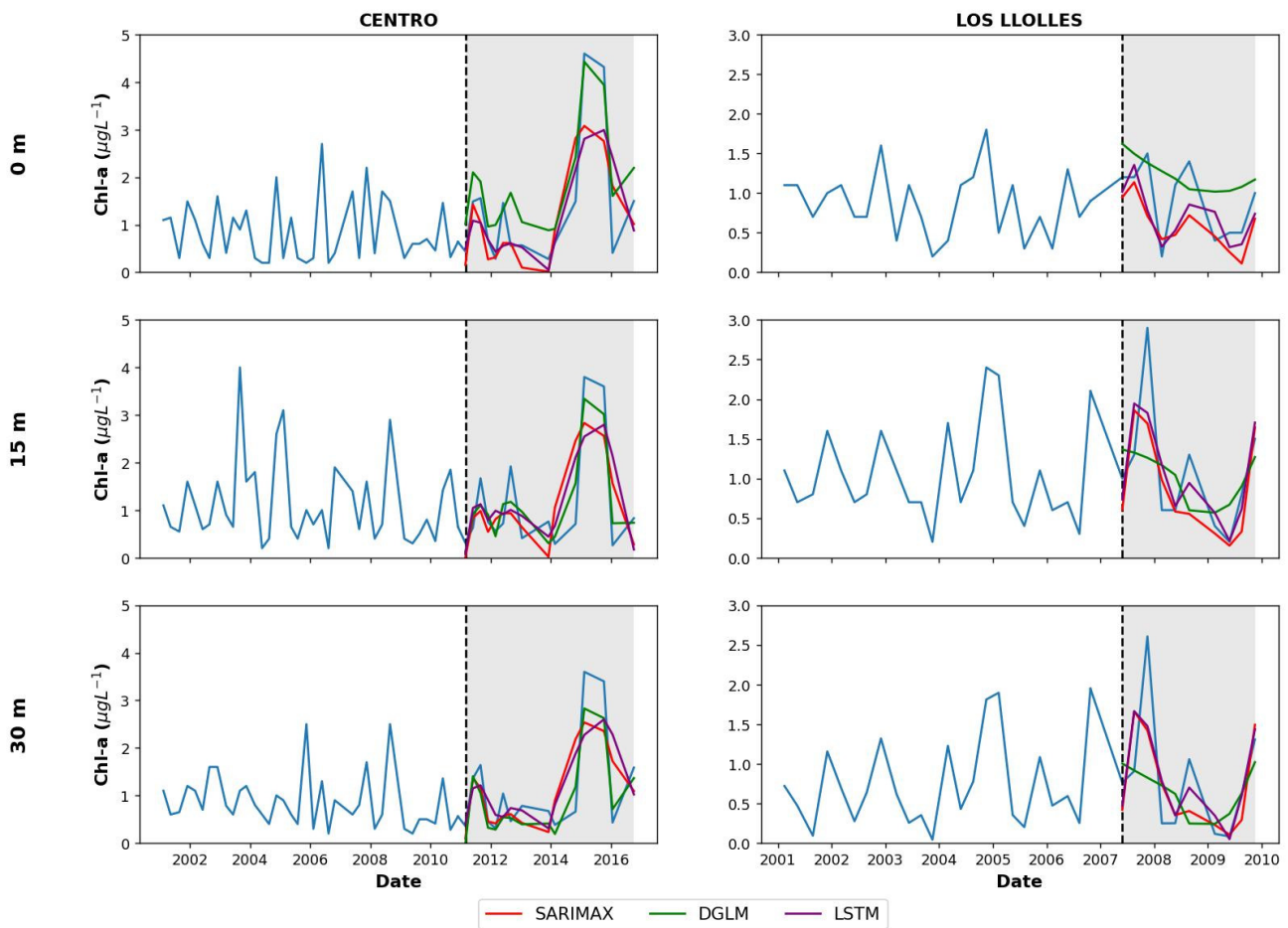


**Figure 10.** Chlorophyll-a estimation for Scenario 3.2 in the two sampling stations with data from Maihue Lake during 2001–2016. The shaded regions represent observations for the selection of the test.

**Table 7.** Validation metrics for all the stations and models considered in Scenario 3.2.

| Model/Station | Station     | Depth | MSE<br>( $\mu\text{g/L}$ ) <sup>2</sup> | RMSE<br>( $\mu\text{g/L}$ ) | MaxError<br>( $\mu\text{g/L}$ ) | MAE<br>( $\mu\text{g/L}$ ) | R <sup>2</sup> |
|---------------|-------------|-------|---|-----------------------------|---------------------------------|----------------------------|----------------|
| SARIMAX       | CENTRO      | 0 m   | 0.69                                    | 0.82                        | 2.67                            | 0.91                       | 0.30           |
|               |             | 15 m  | 0.67                                    | 0.82                        | 2.43                            | 0.98                       | 0.32           |
|               |             | 30 m  | 0.59                                    | 0.71                        | 2.42                            | 0.98                       | 0.36           |
|               | LOS LLOLLES | 0 m   | 0.19                                    | 0.43                        | 0.79                            | 0.35                       | 0.35           |
|               |             | 15 m  | 0.29                                    | 0.54                        | 1.21                            | 0.41                       | 0.47           |
|               |             | 30 m  | 0.32                                    | 0.57                        | 1.29                            | 0.42                       | 0.39           |
| DGLM          | CENTRO      | 0 m   | 0.42                                    | 0.65                        | 1.19                            | 0.57                       | 0.75           |
|               |             | 15 m  | 0.22                                    | 0.47                        | 0.85                            | 0.41                       | 0.82           |
|               |             | 30 m  | 0.17                                    | 0.42                        | 0.77                            | 0.34                       | 0.83           |
|               | LOS LLOLLES | 0 m   | 0.26                                    | 0.51                        | 1.07                            | 0.42                       | 0.38           |
|               |             | 15 m  | 0.35                                    | 0.59                        | 1.40                            | 0.39                       | 0.46           |
|               |             | 30 m  | 0.48                                    | 0.69                        | 1.88                            | 0.44                       | 0.48           |



Table 7. Cont.

| Model/Station | Station     | Depth | MSE<br>( $\mu\text{g/L}$ ) <sup>2</sup> | RMSE<br>( $\mu\text{g/L}$ ) | MaxError<br>( $\mu\text{g/L}$ ) | MAE<br>( $\mu\text{g/L}$ ) | R <sup>2</sup> |
|---------------|-------------|-------|---|-----------------------------|---------------------------------|----------------------------|----------------|
| LSTM          | CENTRO      | 0 m   | 0.74                                    | 0.86                        | 2.01                            | 0.59                       | 0.57           |
|               |             | 15 m  | 0.68                                    | 0.82                        | 1.88                            | 0.66                       | 0.44           |
|               |             | 30 m  | 0.59                                    | 0.76                        | 1.85                            | 0.59                       | 0.46           |
|               | LOS LLOLLES | 0 m   | 0.15                                    | 0.38                        | 1.04                            | 0.24                       | 0.42           |
|               |             | 15 m  | 0.22                                    | 0.47                        | 1.08                            | 0.36                       | 0.59           |
|               |             | 30 m  | 0.24                                    | 0.49                        | 1.13                            | 0.36                       | 0.57           |

#### 4. Discussion

The remote lakes of the Andes have long been an enigma in terms of historical information on the limnological characteristics of their waters. In this context, our study of Lake Maihue has emerged as a beacon of knowledge, allowing us to obtain valuable data on the current state of water quality and the evolution of its algal community. Our approach involved an assessment through three different scenarios: Scenario 1 (field measurement data), Scenario 2 (meteorological data), and Scenario 3 (satellite data). Through these scenarios, we have employed three deep learning and traditional statistical models to estimate the behavior of the variable Chl-a, taking advantage of the richness of data offered by these parameters. The models used for the estimation of Chl-a, SARIMAX, DGLM, and LSTM, have proven their effectiveness in various applications and were successfully employed in our study.

From the results obtained, we can observe that Scenario 2 exhibits better performance metrics, with lower MSE/RMSE values and higher R<sup>2</sup> scores than the other ones, with both LSTM and DGLM as the best models across various stations and depths. Scenario 1, on the contrary, although also presenting low MSE and RMSE values, generally exhibits slightly lower R<sup>2</sup> scores than those in Scenario 2. Additionally, Scenarios 3.1 and 3.2 showed slightly higher MSE and RMSE values compared to Scenarios 1 and 2. Overall, DGLM and LSTM consistently demonstrated better performance regarding the depths and stations analyzed. In contrast, the SARIMAX performance was the worst, probably due to the difficulties in dealing with non-linearities present in the test data. DGLM and LSTM appear particularly effective in cases involving non-stationary time series, a common characteristic among the series in this study. Notably, the performance tends to improve with increasing depth, with notably better metrics at 15 m. The results obtained have shed light on the superior performance of Scenario 2, supported by more favorable metrics such as lower MSE/RMSE values and higher R<sup>2</sup> scores (see Tables 2–5). In this scenario, LSTM and DGLM stand out as the outstanding models not only at one but also at multiple stations and depths.

Overall, the DLGM model demonstrates superior performance at the CENTRO station, whereas LSTM excels at the LOS LLOLLES station. This outcome aligns with expectations, given the presence of significant outliers in the test data that were not observed in the training data. It is noteworthy that SARIMAX, unlike the DLGM and LSTM models, is limited in its ability to handle such non-linearities.

In addition, it is relevant to mention that the performance tends to improve as depth increases, with significantly more favorable metrics at 15 m depth, where a higher concentration of Chl-a is observed, indicating the presence of algae.

The results of our study reveal that Lake Maihue has experienced a slight increase in Chl-a concentration during the study period, which spans from 2001 to 2020. Our work is part of a series of investigations carried out in lakes in the Chilean mountain range, in which the evolution of algal activity has been closely followed. For example, in a previous study [13] in Lake Laja, the phenomenon of algal blooms was documented. Likewise, another recent study [15] in Lake Villarrica identified a close relationship between these blooms and changing meteorological conditions, directly related to algal blooms. In Lake Llanquihue, artificial intelligence models were tested to estimate the concentration of

chlorophyll-a before other parameters because several regional capitals are in this lake, which contribute to accelerating the impacts on the water quality of this lake system with the multiple uses of this aquatic ecosystem.

Remote sensing has proven to be a valuable tool in the monitoring of lake systems in the mountain range of this South American country and a relevant element in the monitoring of the current state of the water resource as well as the evolution of algae. In this research, the best predictions were obtained with meteorological data rather than satellite data, but this may be a consequence of the insufficient spatial distribution of in situ data. Therefore, in future research, it is intended to have more monitoring stations and carry out modeling with the greatest amount of combined data, including in situ, meteorological, and satellite data in the same model. Our future projection in this direction is to increase the data on water quality parameters and, thus, improve the prediction of deep learning models using a combination of remote sensing data, meteorological data, and field campaigns. Caring for lake water quality is essential to protecting human health, biodiversity, the local economy, and the environment in general. It is vital to take measures to prevent pollution and promote sustainable management of these valuable water resources.

## 5. Conclusions

The employment of in situ, meteorological, and remote sensing data has been highlighted as a valuable resource for estimating environmental indicators, such as chlorophyll-a at different depths. This parameter has been widely used in various aquatic ecosystems to assess both algal biomass and water quality, but at depth, it is a novel contributor. In this study, a set of in situ data collected between 2001 and 2020 at two monitoring stations in Lake Maihue was used to analyze the behavior of limnological variables in different areas of the lake.

The results of this study revealed that the three estimation models used demonstrated an effective ability to predict chlorophyll-a concentration, with the LSTM and DGLM models standing out as the most accurate ones compared to the SARIMAX model.

Of the four scenarios evaluated in this study, Scenario 2 exhibits better performance metrics, yielding the most accurate results for the analyzed stations and depths in the lake. These models will be fundamental tools for future research, especially during the autumn and winter seasons, when episodes of rain and strong winds, such as the Puelches winds, are common and conventional monitoring is more complex. Consequently, there is a need to use estimation models, such as those presented in this study, that combine real data with meteorological and remote sensing data using deep learning tools.

**Supplementary Materials:** The following supporting information can be downloaded at <https://www.mdpi.com/article/10.3390/rs16040647/s1>, Table S1: Limnological parameters in the summer season, Table S2: Limnological parameters in the autumn season, Table S3: Limnological parameters in the winter season, and Table S4: Limnological parameters in the spring season.

**Author Contributions:** Conceptualization, L.R.-L.; methodology, L.R.-L. and D.B.U.; software, L.R.-L., D.B.U. and I.D.-L.; validation, L.B.A, L.R.-L. and D.B.U.; formal analysis, L.R.-L.; investigation, L.R.-L. and D.B.U.; resources, R.U., L.R.-L. and D.B.U.; data curation, L.R.-L. and D.B.U.; writing—original draft preparation, L.R.-L. and D.B.U.; writing—review and editing, L.R.-L., D.B.U., D.A., I.D.-L.; N.F., F.F. and L.B.; visualization, L.B.A. and I.D.-L.; supervision, R.U. and F.F.; project administration, L.R.-L. and D.B.U.; funding acquisition, L.R.-L., D.A., L.B. and F.F. All authors have read and agreed to the published version of the manuscript.

**Funding:** This research was funded by “Proyecto Interuniversitario de Iniciación en Investigación Asociativa: P3IA-22/23” and Vicerrectoría de Investigación y Doctorados Universidad San Sebastián.

**Data Availability Statement:** The data presented in this study are available upon request from the corresponding author.

**Acknowledgments:** L.R.-L. and D.A. thank the “Proyecto Interuniversitario de Iniciación en Investigación Asociativa: P3IA-22/23”, and L.R.-L. is grateful to the Centro de Recursos Hídricos para la

Agricultura y la Minería (CRHIAM) (Project ANID/FONDAP/15130015 and ANID/FONDAP/1523A0001). D.A. thanks Fondecyt Iniciación 11201231.

**Conflicts of Interest:** The authors declare no conflicts of interest.

## References

- Moser, K.A.; Baron, J.S.; Brahney, J.; Oleksy, I.A.; Saros, J.E.; Hundey, E.J.; Sadro, S.A.; Kopáček, J.; Sommaruga, R.; Kainz, M.J.; et al. Mountain Lakes: Eyes on Global Environmental Change. *Glob. Planet. Change* **2019**, *178*, 77–95. [[CrossRef](#)]
- Tong, H.-L.; Shi, P.-J. Using Ecosystem Service Supply and Ecosystem Sensitivity to Identify Landscape Ecology Security Patterns in the Lanzhou-Xining Urban Agglomeration, China. *J. Mt. Sci.* **2020**, *17*, 2758–2773. [[CrossRef](#)]
- Grebby, S.; Sowter, A.; Gee, D.; Athab, A.; De la Barreda-Bautista, B.; Girindran, R.; Marsh, S. Remote Monitoring of Ground Motion Hazards in High Mountain Terrain Using InSAR: A Case Study of the Lake Sarez Area, Tajikistan. *Appl. Sci.* **2021**, *11*, 8738. [[CrossRef](#)]
- Regmi, G.R.; Huettmann, F. *Hindu Kush-Himalaya Watersheds Downhill: Landscape Ecology and Conservation Perspectives*; Springer International Publishing: Cham, Switzerland, 2020; ISBN 9783030362751.
- Wolf, I.D.; Croft, D.B.; Green, R.J. Nature Conservation and Nature-Based Tourism: A Paradox? *Environments* **2019**, *6*, 104. [[CrossRef](#)]
- Danilov-Danilyan, V.I.; Klyuev, N.N.; Kotlyakov, V.M. Russia in the Global Natural and Ecological Space. *Reg. Res. Russ.* **2023**, *13*, 34–57. [[CrossRef](#)]
- Paltsev, A.; Creed, I.F. Are Northern Lakes in Relatively Intact Temperate Forests Showing Signs of Increasing Phytoplankton Biomass? *Ecosystems* **2021**, *25*, 727–755. [[CrossRef](#)]
- Pritsch, H.; Schirpke, U.; Jersabek, C.D.; Kurmayer, R. Plankton Community Composition in Mountain Lakes and Consequences for Ecosystem Services. *Ecol. Indic.* **2023**, *154*, 110532. [[CrossRef](#)]
- De los Ríos-Escalante, P.R.; Woelfl, S. A Review of Zooplankton Research in Chile. *Limnologica* **2023**, *100*, 126079. [[CrossRef](#)]
- Tovar-Sánchez, A.; Román, A.; Roque-Atienza, D.; Navarro, G. Applications of Unmanned Aerial Vehicles in Antarctic Environmental Research. *Sci. Rep.* **2021**, *11*, 21717. [[CrossRef](#)] [[PubMed](#)]
- Kallenbach, E.M.F.; Friberg, N.; Lusher, A.; Jacobsen, D.; Hurley, R.R. Anthropogenically Impacted Lake Catchments in Denmark Reveal Low Microplastic Pollution. *Environ. Sci. Pollut. Res.* **2022**, *29*, 47726–47739. [[CrossRef](#)] [[PubMed](#)]
- Cantonati, M.; Poikane, S.; Pringle, C.M.; Stevens, L.E.; Turak, E.; Heino, J.; Richardson, J.S.; Bolpagni, R.; Borrini, A.; Cid, N.; et al. Characteristics, Main Impacts, and Stewardship of Natural and Artificial Freshwater Environments: Consequences for Biodiversity Conservation. *Water* **2020**, *12*, 260. [[CrossRef](#)]
- Rodríguez-López, L.; Duran-Llacer, I.; González-Rodríguez, L.; Abarca-del-Rio, R.; Cárdenas, R.; Parra, O.; Martínez-Retureta, R.; Urrutia, R. Spectral Analysis Using LANDSAT Images to Monitor the Chlorophyll-a Concentration in Lake Laja in Chile. *Ecol. Inform.* **2020**, *60*, 101183. [[CrossRef](#)]
- Rodríguez-López, L.; Usta, D.B.; Duran-Llacer, I.; Alvarez, L.B.; Yépez, S.; Bourel, L.; Frappart, F.; Urrutia, R. Estimation of Water Quality Parameters through a Combination of Deep Learning and Remote Sensing Techniques in a Lake in Southern Chile. *Remote Sens.* **2023**, *15*, 4157. [[CrossRef](#)]
- Rodríguez-López, L.; Duran-Llacer, I.; Bravo Alvarez, L.; Lami, A.; Urrutia, R. Recovery of Water Quality and Detection of Algal Blooms in Lake Villarrica through Landsat Satellite Images and Monitoring Data. *Remote Sens.* **2023**, *15*, 1929. [[CrossRef](#)]
- Rodríguez-López, L.; Bustos Usta, D.; Bravo Alvarez, L.; Duran-Llacer, I.; Lami, A.; Martínez-Retureta, R.; Urrutia, R. Machine Learning Algorithms for the Estimation of Water Quality Parameters in Lake Llanquihue in Southern Chile. *Water* **2023**, *15*, 1994. [[CrossRef](#)]
- Park, J.; Kim, K.T.; Lee, W.H. Recent Advances in Information and Communications Technology (ICT) and Sensor Technology for Monitoring Water Quality. *Water* **2020**, *12*, 510. [[CrossRef](#)]
- Rodríguez-López, L.; González-Rodríguez, L.; Duran-Llacer, I.; Cardenas, R.; Urrutia, R. Spatio-Temporal Analysis of Chlorophyll in Six Araucanian Lakes of Central-South Chile from Landsat Imagery. *Ecol. Inform.* **2021**, *65*, 101431. [[CrossRef](#)]
- Skakun, S.; Kalecinski, N.I.; Brown, M.G.L.; Johnson, D.M.; Vermote, E.F.; Roger, J.C.; Franch, B. Assessing Within-Field Corn and Soybean Yield Variability from Worldview-3, Planet, Sentinel-2, and Landsat 8 Satellite Imagery. *Remote Sens.* **2021**, *13*, 872. [[CrossRef](#)]
- Vrdoljak, L.; Kilić Pamuković, J. Assessment of Atmospheric Correction Processors and Spectral Bands for Satellite-Derived Bathymetry Using Sentinel-2 Data in the Middle Adriatic. *Hydrology* **2022**, *9*, 215. [[CrossRef](#)]
- Legleiter, C.J.; King, T.V.; Carpenter, K.D.; Hall, N.C.; Mumford, A.C.; Slonecker, T.; Graham, J.L.; Stengel, V.G.; Simon, N.; Rosen, B.H. Spectral Mixture Analysis for Surveillance of Harmful Algal Blooms (SMASH): A Field-, Laboratory-, and Satellite-Based Approach to Identifying Cyanobacteria Genera from Remotely Sensed Data. *Remote Sens. Environ.* **2022**, *279*, 113089. [[CrossRef](#)]
- de Lima, T.M.A.; Giardino, C.; Bresciani, M.; Barbosa, C.C.F.; Fabbretto, A.; Pellegrino, A.; Begliomini, F.N. Assessment of Estimated Phycocyanin and Chlorophyll-a Concentration from PRISMA and OLCI in Brazilian Inland Waters: A Comparison between Semi-Analytical and Machine Learning Algorithms. *Remote Sens.* **2023**, *15*, 1299. [[CrossRef](#)]
- Zhang, H.; Xue, B.; Wang, G.; Zhang, X.; Zhang, Q. Deep Learning-Based Water Quality Retrieval in an Impounded Lake Using Landsat 8 Imagery: An Application in Dongping Lake. *Remote Sens.* **2022**, *14*, 4505. [[CrossRef](#)]

24. Gómez, D.; Salvador, P.; Sanz, J.; Casanova, J.L. A New Approach to Monitor Water Quality in the Menor Sea (Spain) Using Satellite Data and Machine Learning Methods. *Environ. Pollut.* **2021**, *286*, 117489. [[CrossRef](#)] [[PubMed](#)]
25. Chusnah, W.N.; Chu, H.J.; Tatas; Jaelani, L.M. Machine-Learning-Estimation of High-Spatiotemporal-Resolution Chlorophyll-a Concentration Using Multi-Satellite Imagery. *Sustain. Environ. Res.* **2023**, *33*, 11. [[CrossRef](#)]
26. Medina-López, E.; Navarro, G.; Santos-Echeandía, J.; Bernárdez, P.; Caballero, I. Machine Learning for Detection of Macroalgal Blooms in the Mar Menor Coastal Lagoon Using Sentinel-2. *Remote Sens.* **2023**, *15*, 1208. [[CrossRef](#)]
27. Berger, K.; Rivera Caicedo, J.P.; Martino, L.; Woche, M.; Hank, T.; Verrelst, J. A Survey of Active Learning for Quantifying Vegetation Traits from Terrestrial Earth Observation Data. *Remote Sens.* **2021**, *13*, 287. [[CrossRef](#)] [[PubMed](#)]
28. Nasir, N.; Kansal, A.; Alshaltone, O.; Barneih, F.; Shanableh, A.; Al-Shabi, M.; Al Shammaa, A. Deep Learning Detection of Types of Water-Bodies Using Optical Variables and Ensembling. *Intell. Syst. Appl.* **2023**, *18*, 200222. [[CrossRef](#)]
29. Sadaippan, B.; Balakrishnan, P.; Vishal, C.R.; Vijayan, N.T.; Subramanian, M.; Gauns, M.U. Applications of Machine Learning in Chemical and Biological Oceanography. *ACS Omega* **2023**, *8*, 15831–15853. [[CrossRef](#)] [[PubMed](#)]
30. Peterson, K.T.; Sagan, V.; Sidike, P.; Hasenmueller, E.A.; Sloan, J.J.; Knouft, J.H. Machine Learning-Based Ensemble Prediction of Water-Quality Variables Using Feature-Level and Decision-Level Fusion with Proximal Remote Sensing. *Photogramm. Eng. Remote Sens.* **2019**, *85*, 269–280. [[CrossRef](#)]
31. Heng, Y.; Wai, K.; Shen, B.; Chun, A.; Loy, M.; Shahbaz, M.; Kaur, H.; Singh, G.; Yusuf, R.; Fadzil, A.; et al. Science of the Total Environment An Overview of Biomass Thermochemical Conversion Technologies in Malaysia. *Sci. Total Environ.* **2019**, *680*, 105–123. [[CrossRef](#)]
32. Pahlevan, N.; Smith, B.; Schalles, J.; Binding, C.; Cao, Z.; Ma, R.; Alikas, K.; Kangro, K.; Gurlin, D.; Hà, N.; et al. Seamless Retrievals of Chlorophyll-a from Sentinel-2 (MSI) and Sentinel-3 (OLCI) in Inland and Coastal Waters: A Machine-Learning Approach. *Remote Sens. Environ.* **2020**, *240*, 111604. [[CrossRef](#)]
33. Su, H.; Lu, X.; Chen, Z.; Zhang, H.; Lu, W.; Wu, W. Estimating Coastal Chlorophyll-a Concentration from Time-Series Olci Data Based on Machine Learning. *Remote Sens.* **2021**, *13*, 576. [[CrossRef](#)]
34. Li, H.; Qin, C.; He, W.; Sun, F.; Du, P. Improved Predictive Performance of Cyanobacterial Blooms Using a Hybrid Statistical and Deep-Learning Method. *Environ. Res. Lett.* **2021**, *16*, 124045. [[CrossRef](#)]
35. Nguyen, H.Q.; Ha, N.T.; Nguyen-Ngoc, L.; Pham, T.L. Comparing the Performance of Machine Learning Algorithms for Remote and in Situ Estimations of Chlorophyll-a Content: A Case Study in the Tri an Reservoir, Vietnam. *Water Environ. Res.* **2021**, *93*, 2941–2957. [[CrossRef](#)]
36. Kolluru, S.; Tiwari, S.P. Modeling Ocean Surface Chlorophyll-a Concentration from Ocean Color Remote Sensing Reflectance in Global Waters Using Machine Learning. *Sci. Total Environ.* **2022**, *844*, 157191. [[CrossRef](#)]
37. Bartold, M.; Kluczek, M. A Machine Learning Approach for Mapping Chlorophyll Fluorescence at Inland Wetlands. *Remote Sens.* **2023**, *15*, 2392. [[CrossRef](#)]
38. Caballero, I.; Fernández, R.; Escalante, O.M.; Mamán, L.; Navarro, G. New Capabilities of Sentinel-2A/B Satellites Combined with in Situ Data for Monitoring Small Harmful Algal Blooms in Complex Coastal Waters. *Sci. Rep.* **2020**, *10*, 8743. [[CrossRef](#)]
39. Zheng, L.; Wang, H.; Liu, C.; Zhang, S.; Ding, A.; Xie, E.; Li, J.; Wang, S. Prediction of Harmful Algal Blooms in Large Water Bodies Using the Combined EFDC and LSTM Models. *J. Environ. Manag.* **2021**, *295*, 113060. [[CrossRef](#)]
40. De Los Rios-Escalante, P.; Woelfl, S. Use of Null Models to Explain Crustacean Zooplankton Assemblages in North Patagonian Lakes with Presence or Absence of Mixotrophic Ciliates (38°S, Chile). *Crustaceana* **2017**, *90*, 311–319. [[CrossRef](#)]
41. Van Daele, M.; Moernaut, J.; Doom, L.; Boes, E.; Fontijn, K.; Heirman, K.; Vandoorne, W.; Hebbeln, D.; Pino, M.; Urrutia, R.; et al. A Comparison of the Sedimentary Records of the 1960 and 2010 Great Chilean Earthquakes in 17 Lakes: Implications for Quantitative Lacustrine Palaeoseismology. *Sedimentology* **2015**, *62*, 1466–1496. [[CrossRef](#)]
42. Woelfl, S. The Distribution of Large Mixotrophic Ciliates (Stentor) in Deep North Patagonian Lakes (Chile): First Results. *Limnologia* **2007**, *37*, 28–36. [[CrossRef](#)]
43. Kelly, S. Megawatts Mask Impacts: Small Hydropower and Knowledge Politics in the Puelwillimapu, Southern Chile. *Energy Res. Soc. Sci.* **2019**, *54*, 224–235. [[CrossRef](#)]
44. Rodríguez-López, L.; González-Rodríguez, L.; Duran-Llacer, I.; García, W.; Cardenas, R.; Urrutia, R. Assessment of the Diffuse Attenuation Coefficient of Photosynthetically Active Radiation in a Chilean Lake. *Remote Sens.* **2022**, *14*, 4568. [[CrossRef](#)]
45. Chatenoux, B.; Richard, J.P.; Small, D.; Roeoesli, C.; Wingate, V.; Poussin, C.; Rodila, D.; Peduzzi, P.; Steinmeier, C.; Ginzler, C.; et al. The Swiss Data Cube, Analysis Ready Data Archive Using Earth Observations of Switzerland. *Sci. Data* **2021**, *8*, 295. [[CrossRef](#)]
46. Vanhellemont, Q.; Ruddick, K. Atmospheric Correction of Metre-Scale Optical Satellite Data for Inland and Coastal Water Applications. *Remote Sens. Environ.* **2018**, *216*, 586–597. [[CrossRef](#)]
47. Vanhellemont, Q. Adaptation of the Dark Spectrum Fitting Atmospheric Correction for Aquatic Applications of the Landsat and Sentinel-2 Archives. *Remote Sens. Environ.* **2019**, *225*, 175–192. [[CrossRef](#)]
48. Vanhellemont, Q. Sensitivity Analysis of the Dark Spectrum Fitting Atmospheric Correction for Metre- and Decametre-Scale Satellite Imagery Using Autonomous Hyperspectral Radiometry. *Opt Express* **2020**, *28*, 29948. [[CrossRef](#)]
49. Vanhellemont, Q.; Ruddick, K. Turbid Wakes Associated with Offshore Wind Turbines Observed with Landsat 8. *Remote Sens. Environ.* **2014**, *145*, 105–115. [[CrossRef](#)]

50. Vanhellemont, Q.; Ruddick, K. Advantages of High Quality SWIR Bands for Ocean Colour Processing: Examples from Landsat-8. *Remote Sens. Environ.* **2015**, *161*, 89–106. [[CrossRef](#)]
51. Vanhellemont, Q.; Ruddick, K. Acolite for Sentinel-2: Aquatic Applications of Msi Imagery. In Proceedings of the 2016 ESA Living Planet Symposium, Prague, Czech Republic, 9–13 May 2016.
52. Rodríguez-López, L.; Duran-Llacer, I.; González-Rodríguez, L.; Cardenas, R.; Urrutia, R. Retrieving Water Turbidity in Araucanian Lakes (South-Central Chile) Based on Multispectral Landsat Imagery. *Remote Sens.* **2021**, *13*, 3133. [[CrossRef](#)]
53. Werther, M.; Odermatt, D.; Simis, S.G.H.; Gurlin, D.; Lehmann, M.K.; Kutser, T.; Gupana, R.; Varley, A.; Hunter, P.D.; Tyler, A.N.; et al. A Bayesian Approach for Remote Sensing of Chlorophyll-a and Associated Retrieval Uncertainty in Oligotrophic and Mesotrophic Lakes. *Remote Sens. Environ.* **2022**, *283*, 113295. [[CrossRef](#)]
54. Xu, D.; Pu, Y.; Zhu, M.; Luan, Z.; Shi, K. Automatic Detection of Algal Blooms Using Sentinel-2 MSI and Landsat OLI Images. *IEEE J. Sel. Top. Appl. Earth Obs. Remote Sens.* **2021**, *14*, 8497–8511. [[CrossRef](#)]
55. Gitelson, A.A.; Kaufman, Y.J.; Merzlyak, M.N.; Blaustein, J. Use of a Green Channel in Remote Sensing of Global Vegetation from EOS-MODIS. *Remote Sens. Environ.* **1996**, *58*, 289–298. [[CrossRef](#)]
56. Setiawan, F.; Matsushita, B.; Hamzah, R.; Jiang, D.; Fukushima, T. Long-Term Change of the Secchi Disk Depth in Lake Maninjau, Indonesia Shown by Landsat TM and ETM+ Data. *Remote Sens.* **2019**, *11*, 2875. [[CrossRef](#)]
57. Absalon, D.; Matysik, M.; Woźnica, A.; Janczewska, N. Detection of Changes in the Hydrobiological Parameters of the Oder River during the Ecological Disaster in July 2022 Based on Multi-Parameter Probe Tests and Remote Sensing Methods. *Ecol. Indic.* **2023**, *148*, 110103. [[CrossRef](#)]
58. Kowe, P.; Ncube, E.; Magidi, J.; Ndambuki, J.M.; Rwasoka, D.T.; Gumindoga, W.; Maviza, A.; de Jesus Paulo Mavaringana, M.; Kakanda, E.T. Spatial-Temporal Variability Analysis of Water Quality Using Remote Sensing Data: A Case Study of Lake Manyame. *Sci. Afr.* **2023**, *21*, e01877. [[CrossRef](#)]
59. Rouse, J.W.; Haas, R.H.; Schell, J.A.; Deering, D.W. Monitoring Vegetation Systems in the Great Plains with ERTS. *NASA Spec. Publ.* **1974**, *351*, 309–310.
60. Yin, Z.; Li, J.; Zhang, B.; Liu, Y.; Yan, K.; Gao, M.; Xie, Y.; Zhang, F.; Wang, S. Increase in Chlorophyll-a Concentration in Lake Taihu from 1984 to 2021 Based on Landsat Observations. *Sci. Total Environ.* **2023**, *873*, 162168. [[CrossRef](#)]
61. Alawadi, F. Detection of Surface Algal Blooms Using the Newly Developed Algorithm Surface Algal Bloom Index (SABI). *Remote Sens. Ocean. Sea Ice Large Water Reg.* **2010**, *7825*, 782506. [[CrossRef](#)]
62. Hu, C. A Novel Ocean Color Index to Detect Floating Algae in the Global Oceans. *Remote Sens. Environ.* **2009**, *113*, 2118–2129. [[CrossRef](#)]
63. Ma, J.; Jin, S.; Li, J.; He, Y.; Shang, W. Spatio-Temporal Variations and Driving Forces of Harmful Algal Blooms in Chaohu Lake: A Multi-Source Remote Sensing Approach. *Remote Sens.* **2021**, *13*, 427. [[CrossRef](#)]
64. Markogianni, V.; Kalivas, D.; Petropoulos, G.P.; Dimitriou, E. Estimating Chlorophyll-a of Inland Water Bodies in Greece Based on Landsat Data. *Remote Sens.* **2020**, *12*, 2087. [[CrossRef](#)]
65. Gitelson, A.A.; Viña, A.; Ciganda, V.; Rundquist, D.C.; Arkebauer, T.J. Remote Estimation of Canopy Chlorophyll Content in Crops. *Geophys. Res. Lett.* **2005**, *32*, L08403. [[CrossRef](#)]
66. Hassan, M.A.; Yang, M.; Rasheed, A.; Jin, X.; Xia, X.; Xiao, Y.; He, Z. Time-Series Multispectral Indices from Unmanned Aerial Vehicle Imagery Reveal Senescence Rate in Bread Wheat. *Remote Sens.* **2018**, *10*, 809. [[CrossRef](#)]
67. Korstanje, J. *Advanced Forecasting with Python*; Springer: Berlin/Heidelberg, Germany, 2021.
68. Mahmudimanes, M.; Mirzaee, M.; Dehghan, A.; Bahrampour, A. Forecasts of Cardiac and Respiratory Mortality in Tehran, Iran, Using ARIMAX and CNN-LSTM Models. *Environ. Sci. Pollut. Res.* **2022**, *29*, 28469–28479. [[CrossRef](#)]
69. West, M.; Harrison, P.J.; Migon, H.S. Dynamic Generalized Linear Models and Bayesian Forecasting. *J. Am. Stat. Assoc.* **1985**, *80*, 73–83. [[CrossRef](#)]
70. Hochreiter, S.; Jürgen Schmidhuber, J. Long Short-Term Memory. *Neural Comput.* **1997**, *9*, 1735–1780. [[CrossRef](#)]
71. Yu, Y.; Si, X.; Hu, C.; Zhang, J. A Review of Recurrent Neural Networks: Lstm Cells and Network Architectures. *Neural Comput.* **2019**, *31*, 1235–1270. [[CrossRef](#)]
72. Das, K.; Jiang, J.; Rao, J.N.K. Mean Squared Error of Empirical Predictor. *Ann. Statist.* **2004**, *32*, 818–840. [[CrossRef](#)]
73. Maier, A.K.; Syben, C.; Stimpel, B.; Würfl, T.; Hoffmann, M.; Schebesch, F.; Fu, W.; Mill, L.; Kling, L.; Christiansen, S. Learning with Known Operators Reduces Maximum Error Bounds. *Nat. Mach. Intell.* **2019**, *1*, 373–380. [[CrossRef](#)]
74. Luetkepohl, H. *New Introduction to Multiple Time Series Analysis*; Springer: Berlin/Heidelberg, Germany, 2005.
75. Hyndman, R.J.; Athanasopoulos, G. *Forecasting: Principles and Practice*; Springer: Berlin/Heidelberg, Germany, 2018.
76. Luíza da Costa, N.; Dias de Lima, M.; Barbosa, R. Evaluation of Feature Selection Methods Based on Artificial Neural Network Weights. *Expert Syst. Appl.* **2021**, *168*, 114312. [[CrossRef](#)]

**Disclaimer/Publisher’s Note:** The statements, opinions and data contained in all publications are solely those of the individual author(s) and contributor(s) and not of MDPI and/or the editor(s). MDPI and/or the editor(s) disclaim responsibility for any injury to people or property resulting from any ideas, methods, instructions or products referred to in the content.